Mechanisms required to detach myosin V motors from cargoes

by

Richard G. Yau

A dissertation submitted in partial fulfillment
of the requirements for the degree of
Doctor of Philosophy
(Cellular and Molecular Biology)
in the University of Michigan
2013

Doctoral Committee:
Professor Lois S. Weisman, Chair
Professor Vernon B. Carruthers
Professor Kathleen L. Collins
Professor Daniel J. Klionsky
Professor Kristen J. Verhey

“Sometimes the hardest decisions to make are the easiest to follow”

David Hasselhoff as Mitch Buchannon, Baywatch

Acknowledgements

I thank Dr. Lois Weisman for taking a chance and accepting me into her lab when I had nowhere else to turn to. She has been a great source of encouragement and inspiration. I have learned a great deal about science and life from her. She is genuinely caring and embodies many qualities I strive to attain. I get to write this thesis today thanks to her.

I would like to thank past and present members of the Weisman Lab, Dr. Yui Jin, Dr. Natsuko Jin, Dr. Yanling Zhang, Dr. Sergey Zolov, Michael Lang, Sara Wong, Matthew Brunner and P. Taylor Eves. They have provided many insights into my thesis work. I thank Dr. Mark Hochstrasser (Yale) for kindly providing the E1 and proteasome mutants strains. I thank Dr. Robert Piper (U. of Iowa) for the CUP1-myc-Ub plasmid. I thank Dr. Connie Yutian Peng for identifying Vac17 residues required for the termination of vacuole transport and with Melehia Frauenholtz, isolating the *vac22-1* mutant. I would also like to thank Dr. Rajeshwari Valiathan for her initial characterization of the *vac22-1* mutant. These findings set the foundations for my thesis work. I thank Bethany Strunk for her kind words of encouragement and her genuine interest in my work. I thank Emily Kauffman for being a great colleague and above all else a wonderful person and supportive friend.

I thank my thesis committee members, Dr. Kathleen Collins, Dr. Vernon Carruthers, Dr. Daniel Klionsky and Dr. Kristen Verhey. They have provided deep insights into my work, the guidance to keep my work focused and the encouragement to keep moving forward. I would also like to thank the director of the Cellular and Molecular Biology graduate program, Robert Fuller, for forcing me to graduate.

Lastly, I thank my family and friends. I thank my sister, Lisa Yau, for making me laugh and taking care of things at home while I've been away. I thank my friends for listening to my rants and for their support. Most of grad school has been like walking down a dark tunnel, I wouldn't have made it as far as I have without the love and support of everyone I've met along the way.

Table of contents

List of Tables

List of Figures

Abstract

Establishing the accurate subcellular distribution of organelles is essential for cell function and homeostasis. Transport of organelles to their correct locations by molecular motors is critical for the proper distribution of organelles. Recent studies suggest an unexpected requirement for the accurate detachment of organelles from their associated motors and for the proper deposition of organelles at their correct destinations.

In *Saccharomyces cerevisiae*, in coordination with the cell cycle, organelles are transported from the mother cell to the bud along actin cables. Most cytoplasmic organelles are transported by the myosin V motor, Myo2. Myo2 attaches to organelles via cargo-specific adaptor proteins. For example, Inp2, Mmr1, Vac17 and Ypt31/32, Sec4/Sec15 attach Myo2 to peroxisomes, mitochondria, the vacuole and secretory vesicles respectively. Each cargo has a distinct itinerary. Myo2 orchestrates the transport of diverse organelles in part through the regulated attachment to and detachment from cargoes.

Studies of vacuole transport demonstrate that cargo adaptors play key roles in regulating the transport of organelles. At the start of the cell cycle, the vacuole-specific adaptor, Vac17, is phosphorylated by Cdk1 at four sites. Cdk1 dependent phosphorylation promotes the interaction of Vac17 with Myo2 which attaches Myo2 to the vacuole and initiates vacuole transport in coordination with the start of the cell cycle. Subsequently, the degradation of Vac17 detaches the vacuole from Myo2 and deposits

the vacuole in the bud. The mechanisms which regulate cargo detachment from Myo2 remain poorly understood.

Studies reported here demonstrate that vacuole detachment from Myo2 occurs in multiple regulated steps along the entire pathway of vacuole transport. Detachment initiates in the mother cell with the phosphorylation of Vac17 which recruits the E3 ligase, Dma1, to the vacuole. However, Dma1 recruitment also requires the assembly of the vacuole transport complex and is first observed after the vacuole enters the bud. Dma1 remains on the vacuole until the bud and mother vacuoles separate. Subsequently, Dma1 targets Vac17 for proteasomal degradation. Notably, we find that the termination of peroxisome transport also requires Dma1. We predict that this is a general mechanism which detaches myosin V from select cargoes.

CHAPTER I

Introduction

In eukaryotic cells, organelles are membrane bound subcellular compartments which carry out different cellular processes required for cells to function, respond to external stimuli and maintain homeostasis. While each organelle is a distinct compartment, they are not static sites which carry out isolated cellular processes, rather they are highly dynamic. There is abundant trafficking and communication between organelles to coordinate different processes (Kvam and Goldfarb, 2007; Michel and Kornmann, 2012; Sousa et al., 2011). For some organelles, morphology is regulated via cycles of fusion and fission (Mao and Klionsky, 2013; Rossanese and Glick, 2001; Wickner, 2010). Moreover, it is becoming increasingly clear that the subcellular location of organelles is critical for cell function.

Organelles are often transported to distinct subcellular sites. For example, neuronal plasticity of purkinje neurons requires the transport of the ER into dendritic spines (Wagner et al., 2011). In hippocampal neurons and intestinal epithelia, the recycling of endosomes from intracellular compartments to the cell surface regulates the ability of these cells to respond to external stimuli. Pigmentation requires the transport of pigment containing melanosomes to the periphery of melanocytes and their subsequent transfer to neighboring keratinocytes (Hammer and Sellers, 2011).

In general, long range transport occurs on microtubules via kinesin and dynein motors while short range transport occurs on actin via myosin V motors. Cargoes are

commonly transported to the cell periphery by kinesins and transferred on to myosin to navigate through actin rich networks to reach their final destinations (Wu et al., 1998). Thus, in mammalian cells, organelle transport occurs via the coordinated actions of both microtubule and actin based motors.

In *Saccharomyces cerevisiae*, organelles are also transported to specific subcellular locations. In coordination with the cell cycle, organelles are transported from the mother cell to the bud. Unlike mammalian cells, transport occurs predominantly on actin filaments using myosin V. The directionality of organelle transport is regulated in part through the polarity of actin cables which directs the traffic of myosin V transport into the bud. In addition, the attachment of myosin V to its cargoes is highly regulated which dictates when and where organelle transport initiates. Furthermore, recent studies suggest that the detachment of organelles from myosin is also regulated which deposits organelles at their correct subcellular destinations. Thus, studies of *S. cerevisiae* have uncovered many mechanistic insights into the temporal and spatial regulation of myosin V transport.

Myosin

Myosins comprise a diverse superfamily of motor proteins which are divided into 18 classes (Foth et al., 2006). Most eukaryotic organisms express myosin genes from several classes. Myosin motors convert energy derived from ATP hydrolysis into mechanical force which drives movement along actin cables. In general, myosins consist of 3 main structural domains, the motor domain at the N-terminus, the lever arm and a C-terminal tail domain. The motor domain contains both the actin and nucleotide

binding sites. The motor domain cannot strongly bind ATP and F-actin simultaneously. In the ATP bound state, affinity of the motor domain for F-actin decreases and motor domain releases from actin. In the ADP bound state, affinity of the motor domain for F-actin increases and motor domain binds actin. ATP hydrolysis induces conformational changes in the motor domain which is then amplified by the lever arm into a power stroke and propels the motor forward along actin cables. The lever arm may contain up to six IQ motifs with the sequence IQxxxRGxxxR, where x denotes any amino acid (Terrak et al., 2005). Each IQ motif binds calmodulins or calmodulin-like light chains which stiffens and regulates the lever arm (Trybus, 2008). The tail domain exhibits the greatest degree of diversity between the classes of myosins. This diversity confers distinct functions to different myosins. For example, the tail domains of the conventional class II myosins enable these myosins to oligomerize into bipolar filaments. These myosins are anchored in place while their motor domains move along actin cables which generate a contractile force. In contrast, the tail domains of class V myosins allow these motors to bind and transport cargoes.

Like other myosins, class V myosin motors consist of a motor domain, lever arm and tail. The tail domain contains the rod region and the cargo binding domain (CBD) (Figure 1.1). Two myosin V heavy chains dimerize via their rod regions and function as a homodimer. Coordinated cycles of ATP binding and subsequent hydrolysis of ATP into ADP between the two motor domains enable processive movement along actin. The distance between the two lever arms per myosin V dimer dictates the length of the 72 nm steps along actin. Following the rod region is the CBD which recognizes cargoes. The CBD directly binds cargo specific adaptor proteins which attach myosin V to its

cargoes and initiates cargo transport toward the barbed end of actin filaments (Weisman, 2006).

Establishment of Polarity

In *S. cerevisiae*, organelle transport is coordinated with the cell cycle. Cell division occurs via polarized growth. Organelles and genetic material are targeted from the mother cell to the bud. At the start of the cell cycle, the Ras family GTPase, Rsr1, selects the presumptive bud site on the cell cortex which will eventually develop into the daughter cell. Rsr1 recruits the Rho family GTPase, Cdc42, and its Guanine Exchange Factor (GEF), Cdc24. Active Cdc42 establishes a polarity axis which confines cell growth to the bud site. In the absence of Rsr1, Cdc42/Cdc24 establish polarity at a random site. Cdc42 regulates the polymerization of actin into cortical patches and cables. Actin cortical patches function in endocytosis and their assembly require the actin nucleators, Arp2/3. Actin cables provide the tracks used for polarized secretion and organelle inheritance. Assembly of actin cables is not dependent on Arp2/3. The nucleators for actin cables are the formins Bni1 and Bnr1. Bni1 nucleates actin cables at the bud tip while Bnr1 nucleates cables at the bud neck. Cdc42 recruits Bni1 to the bud tip. Furthermore, Cdc42 with two other Rho family GTPases, Rho3 and Rho4, activate Bni1. Bni1 contains Formin Homology domains FH1 and FH2 which nucleate actin filaments *in vitro*. In budding cells, Bni1 nucleates actin cables which extend from the bud tip deep into the mother cell. The actin cables are polarized with the barbed ends at the bud tip and the pointed ends extending into the mother (Moseley and Goode, 2006; Pruyne and Bretscher, 2000; Pruyne et al., 2004b). Because myosin V is a barbed end

directed motor, the polarity of the actin cables directs the traffic of myosin V transport from the mother cell to the bud tip. Later in the cell cycle, as the size of the bud reaches that of the mother cell, Bni1 is re-localized to the mother-bud neck. The polarity of the actin cables is reversed and directs myosin V transport of secretory vesicles to the site of cytokinesis (Liu et al.; Pruyne et al., 2004a).

Cargo transport

In *S. cerevisiae*, Myo2 transports secretory vesicles, the late Golgi, peroxisomes, the vacuole/lysosome, mitochondria and microtubules. Myo4 transports the Endoplasmic reticulum (ER) and mRNA (Figure 1.2). The myosin V CBD directly binds cargo-specific adaptor proteins which attach myosin V to different cargoes.

Secretory vesicles

A role for Myo2 in organelle transport was first recognized with the identification of the temperature sensitive mutant *myo2-66*. *myo2-66* contains a single missense mutation in the motor domain, E511K (Lillie and Brown, 1994). This mutation would be predicted to impair the transport of Myo2 cargoes. Indeed, at the restrictive temperature of 36^{O}C, secretory vesicles accumulate inside cells. These studies provided evidence implicating that Myo2 transports secretory vesicles (Johnston et al., 1991).

Secretory and membrane proteins modified in the Golgi are packaged into secretory vesicles and transported to the plasma membrane for exocytosis. Secretory vesicles are tethered to the plasma membrane via the exocyst complex. Subsequently, the vesicles fuse with the plasma membrane and release their contents from the cell. The formation of secretory vesicles requires the Rab GTPases, Ypt31/32. Ypt31/32

recruits Sec2, the GEF for the Rab GTPase Sec4. Sec2 then recruits Sec4 to the secretory vesicle and also binds Sec15, a subunit of the exocyst complex. Via Sec2, Sec4 exchanges GDP for GTP and in turn, Sec15 binds activated Sec4. Moreover, Sec4 promotes assembly of the exocyst complex (Guo et al., 1999). Activated Sec4 along with Sro7 and Sec9 mediate the fusion of the secretory vesicles with the plasma membrane (Brennwald et al., 1994; Grosshans et al., 2006). Notably, Myo2 directly interacts with Ypt31/32, Sec4 and Sec15, which attach Myo2 to secretory vesicles during vesicle formation, transport, tethering and fusion with the plasma membrane (Jin et al., 2011; Lipatova et al., 2008; Santiago-Tirado et al., 2011).

Peroxisomes

Peroxisomes function in the metabolism of lipids and reactive oxygen species (ROS). In yeast, a population of peroxisomes is localized to static positions on the cell cortex. In coordination with the cell cycle, a subset of peroxisomes undergoes Myo2 dependent transport into the bud. Peroxisomes are attached to Myo2 via the integral membrane protein and peroxisome specific adaptor, Inp2. In the *inp2*Δ mutant, the bud fails to inherit peroxisomes (Fagarasanu et al., 2006). A recent study identified a second peroxisomal protein, Pex19, which also directly interacts with Myo2. Furthermore, this interaction is critical for peroxisome inheritance (Otzen et al.). Thus, Inp2 and Pex19 function in the attachment of peroxisomes to Myo2.

Vacuole

The yeast vacuole, analogous to the mammalian lysosome, is the site of degradative processes, ion/metabolite/amino acid storage, intracellular pH and osmotic regulation. The vacuole is attached to Myo2 via a protein complex that contains Vac8

and Vac17. Vac8 is anchored to the vacuole membrane via myristoylation and palmitoylation. Vac8 functions in multiple vacuolar processes including, cytoplasm to vacuole protein targeting pathway, formation of the nucleus-vacuole junction, vacuole fusion and vacuole inheritance. Vac8 binds Vac17 and Vac17 directly interacts with Myo2 (Ishikawa et al., 2003; Tang et al., 2003). Assembly of the Myo2/Vac17/Vac8 complex attaches Myo2 to the vacuole and initiates transport. Unlike Vac8, the only function identified for Vac17, is that of a cargo adaptor for Myo2.

Mitochondria

Mitochondria are sites for cellular respiration and energy production. As with other organelles, mitochondria are partitioned into the bud in coordination with the cell cycle. However, the mechanism by which mitochondria move had been largely controversial because two distinct mechanisms had been described. One mechanism is actin dependent and motor independent while the other is actin and motor dependent.

The first mechanism proposes that actin polymerization nucleated by the Arp2/3 complex generates the force which moves mitochondria. This model was based on observations that the Arp2/3 complex associates with the mitochondria and that mutations in the Arp2/3 complex impair mitochondrial movement (Boldogh et al., 2001). In this model, the directionality of transport requires the attachment of mitochondria to actin filaments which extend from the bud tip. Mitochondria are attached to actin filaments via the mitochore complex which consists of Mmm1, Mdm10 and Mdm12 (Boldogh et al., 2003). The mitochore complex attaches to the mitochondria-associated Arp2/3 complex via the RNA binding protein, Puf3 (Garcia-Rodriguez et al., 2007). This model proposes that actin polymerization propels the mitochondria along the actin

cytoskeleton into the bud.

The second mechanism described for mitochondrial transport involves Myo2 and the actin cytoskeleton. Evidence that Myo2 transports mitochondria came from studies which isolated *myo2* mutants, *myo2-338* and *myo2-573*, that cause defects in mitochondrial motility. For *myo2-338*, this defect is likely caused by the loss of the interaction with the Rab GTPase, Ypt11. Further analysis revealed that mitochondrial motility is also impaired in the *ypt11*Δ mutant (Itoh et al., 2002). These observations suggest that Myo2 binds Ypt11 to transport the mitochondria. In an over-expression screen, Mmr1 was identified as a suppressor of *myo2-573*. Furthermore, Mmr1 directly interacted with the Myo2 CBD, localized to the mitochondria and mitochondrial inheritance was impaired in the *mmr1*Δ mutant (Itoh et al., 2004). Time lapse microscopy revealed that in the mmr1Δ mutant, the mitochondria fails to move into the bud (Eves et al., 2012). Together, these observations suggest that Mmr1 is a cargo adaptor for Myo2 and in conjunction with Ypt11, attaches Myo2 to the mitochondria for transport.

Intriguingly, while mitochondrial inheritance is essential, Mmr1 is not. Moreover, the absence of Myo2 based transport causes a delay in mitochondria delivery to bud but does not cause a complete block. These observations are consistent with a model where mitochondrial movement occurs via multiple mechanisms. Because mitochondria are essential organelles that cannot be synthesized *de novo*, multiple pathways may have evolved to ensure that mitochondria are inherited by the bud.

Late Golgi

Secretory and membrane proteins synthesized in the ER are packaged into Coat Protein Complex II (COPII) coated vesicles and undergo anterograde transport to the Golgi complex for modifications before delivery to their final destinations. Conversely, COPI coated vesicles undergo retrograde transport and deliver cargoes from the Golgi complex to the ER. In *S. cerevisiae*, the late Golgi, is transported by Myo2. Ret2, a subunit of the COPI coat, attaches Myo2 to the late Golgi. Ret2 binds Ypt11 which binds the Myo2 CBD (Arai et al., 2008). Similar to the mitochondria, there are other mechanisms that ensure that the bud receives the Golgi. While these other mechanisms have not been studied they likely involve the ability of the late Golgi to form via cisternal maturation (Rossanese and Glick, 2001).

Microtubules

In yeast, spindle pole bodies (SPBs), equivalent to the mammalian centrosome, organize both nuclear and cytoplasmic microtubules (MTs). MTs are polarized with the negative ends at the SPBs and the plus ends extending away from the SPBs. Nuclear MTs attach to the kinetochores of chromosomes and form the mitotic and meiotic spindles. Cytoplasmic MTs attach to the opposite poles of the dividing cell to orient a bipolar spindle which ensures that the proper complement of chromosomes is partitioned between mother and bud (Jaspersen and Winey, 2004). Spindle positioning occurs early in the cell cycle via actin and Myo2 dependent mechanisms (Palmer et al., 1992; Theesfeld et al., 1999; Yin et al., 2000). The MT cargo adaptor, Kar9, associates with SPBs and is then delivered to the plus ends of MTs via binding the MT plus end tracking protein, Bim1 (Lee et al., 2000; Liakopoulos et al., 2003; Miller et al., 2000). Myo2 directly binds Kar9 and transports the plus ends of cytoplasmic MTs to the bud

which orients the spindle. The Myo2-Bim1 fusion protein tracks to the plus ends of MTs and orients the spindle in the absence of Kar9 which suggests that, for spindle positioning, Kar9 functions solely in the attachment of Myo2 to Bim1 (Hwang et al., 2003).

mRNA

Multiple mRNAs are asymmetrically localized to the bud (Shepard et al., 2003). Bud specific mRNAs enable localized protein translation which regulates cell fate determination. While multiple mRNAs are transported to the bud, Asymmetrical Synthesis of HO1 (*ASH1*) mRNA transport is the best characterized. *ASH1* mRNA encodes a transcriptional repressor of the HO endonuclease and suppresses mating type switching (Bobola et al., 1996; Sil and Herskowitz, 1996). Transport of ASH1 mRNA requires Myo4 but not Myo2. Myo4 directly binds She3, She3 binds She2 and She2 directly binds ASH1 mRNA. Fusion of She3 with a high affinity RNA binding domain negates the requirement for She2 in *ASH1* mRNA transport which suggests that the sole role of She2 is to attach Myo4/She3 to ASH1 mRNA (Long et al., 2000). Thus, the She3/She2 complex serves as a cargo adaptor for Myo4.

ER

The endoplasmic reticulum (ER) is the major site for secretory protein synthesis and folding. In *S. cerevisiae*, there are two forms of ER. The perinuclear ER surrounds the nucleus while the cortical ER (cER) localizes to the cell cortex adjacent to the plasma membrane. The cER is the only organelle cargo identified for Myo4. She3, but not She2, attaches the cER to Myo4 (Estrada et al., 2003). Notably, transport of the cER may also occur via a Myo2 dependent mechanism. The Rab GTPase, Ypt11, which

attaches Myo2 to mitochondria and late Golgi, shows extensive co-localization with the ER (Buvelot Frei et al., 2006). Moreover, the ER-mitochondria encounter structures (ERMES) complex mediates points of contacts between the ER and mitochondria. ER-mitochondria contact sites are critical for lipid exchange between the two organelles, protein import to the mitochondria and mitochondrial morphology (Michel and Kornmann, 2012). Thus, Myo2/Ypt11 dependent mitochondrial transport may contribute to ER inheritance via the physical linkages between mitochondria and the ER.

Roles of the myosin V CBD in its attachment to cargoes

Myosin V transports different cargoes to distinct subcellular locations often in coordination with other cellular events such as the cell cycle or in response to external stimuli. To coordinate myosin V transport with other processes, the attachment of myosin V to specific cargoes and the initiation of transport must be tightly regulated. Indeed, many studies have revealed that myosin V transport is regulated via different mechanisms.

One mechanism shown to regulate mammalian myosin V is an auto-inhibition that occurs when an unoccupied CBD binds the motor domain. Differences in closed (inactive) and open (active) conformations can be observed by differential sedimentation. The sedimentation coefficient for activated myosin V is 11S. Inactivation of myosin V changes the sedimentation coefficient to 14S (Ikebe, 2008; Sellers and Knight, 2007). This suggests that inactive myosin V adopts a closed conformation while active myosin V adopts an open conformation. Electron tomography studies revealed that when myosin V is inactive, the CBD folds back and directly interacts with the motor domain, resulting in a more compact form. In the compact conformation, the ATPase

activity of myosin V decreases by ~50-fold compared to myosin V in the extended/active conformation (Lu et al., 2006). Thus, conformational changes directly regulate myosin V transport. It is not yet known whether this mode of regulation occurs for Myo2 or Myo4.

The CBD directly regulates the attachment of myosin V to cargoes. In a forward genetic screen designed to identify mutants that were defective in vacuole inheritance, the mutant *myo2-2* was isolated. *myo2-2* contained a point mutation in its CBD, G1248D, which caused a strong defect in vacuole transport (Catlett and Weisman, 1998). Later studies further identified D1297, L1301, N1304 and N1307 as residues on the Myo2 CBD that directly interacts with Vac17 and are required for vacuole transport (Catlett et al., 2000; Ishikawa et al., 2003). Intriguingly, mutations of any of these residues did not cause growth defects, a phenotype that is associated with impairments in polarized growth. This suggests that these residues are not required for secretory vesicle transport. Conversely, the *myo2-ΔAflII* mutant, with residues 1,459-1,491 deleted from the CBD, is defective in polarized growth but undergoes normal vacuole transport (Catlett and Weisman, 1998). These results suggest that distinct regions on the Myo2 CBD recognize different cargoes. The crystal structure of the Myo2 CBD (residues 1087-1574) revealed that the residues required for secretory vesicle transport and those required for vacuole transport are located in different regions of the CBD (Figure 1.3).

The Myo2 CBD consists of 15 alpha helices connected by loops. The overall structure of the CBD can be separated into two five helical bundles, termed subdomains I and II, and are connected by helix 6. Myo2 residues D1297, L1301, N1304 and N1307, which directly interact with Vac17, all lay on the same surface of helix 6 in subdomain I.

Residues required for secretory vesicle transport, L1331, L1411, Y1415, K1444, and Q1447 are located in subdomain II at a site that is offset by 180^{O} from the region which binds Vac17 (Pashkova et al., 2006).

The crystal structure of the Myo2 CBD and the identification of both the vacuole and secretory vesicle binding sites prompted further studies to identify the binding sites for other Myo2 cargoes. Surprisingly, most cargoes bind the Myo2 CBD at two main regions. The Mmr1 and Vac17 binding sites partially overlap at one region of the CBD. Myo2 residues D1297 and E1293 are required solely for binding Vac17 while residues I1308 and K1312 are required solely for binding Mmr1. However, residues L1229, Q1233, L1301, Y1303, N1304 and N1307 are required for binding both Vac17 and Mmr1 (Figure 1.3). Similarly, the binding sites for Kar9, Inp2, Ypt11, Ypt31/32 and Sec4 partially overlap at a second region of the CBD (Eves et al., 2012). A third binding site was recently identified for Sec15 (Jin et al., 2011). These overlapping binding sites suggest that the binding of the Myo2 CBD to different cargoes is mutually exclusive. Indeed, further analysis of the Vac17 and Mmr1 binding sites demonstrated that these two cargo adaptors compete for access to Myo2 *in vitro* and *in vivo*. Furthermore, this competition regulates the volume of vacuoles and mitochondria that are transported into the bud (Eves et al., 2012). Similar mechanisms may rely on the overlap between the Kar9, Inp2, Ypt11, Ypt31/32 and Sec4 binding sites. Thus, the Myo2 CBD plays critical roles in orchestrating the transport of multiple organelles.

Roles of Cargo Adaptors in the attachment of myosin V to cargoes

Studies of vacuole transport demonstrate that the regulation of a cargo adaptor

contributes to motor-cargo attachment. Vac17 mRNA and protein levels oscillate with the cell cycle (Spellman et al., 1998; Tang et al., 2003). This suggests that the attachment of Myo2 to the vacuole is coordinated with the cell cycle in part via the availability of the vacuole specific adaptor. In addition, Vac17 is regulated via phosphorylation which also oscillates with the cell cycle. The main cyclin dependent kinase, Cdk1, phosphorylates Vac17 at S119, T149, S178 and T248 *in vitro*. Cdk1 dependent phosphorylation promotes the interaction of Vac17 with Myo2 and initiates vacuole transport in coordination with the cell cycle (Peng and Weisman, 2008).

A screen to isolate mutants that are defective in vacuole inheritance revealed that the type 2C serine/threonine protein phosphatase, Ptc1, is required for the transport of multiple Myo2 and Myo4 cargoes. Transport of the vacuole, secretory vesicles, peroxisomes, mitochondria, ER and *ASH1* mRNA are defective in the *ptc1Δ* mutant (Du et al., 2006; Jin et al., 2009; Roeder et al., 1998). In the *ptc1Δ* mutant, Myo2 is partially mis-localized, a phenotype that is also observed in *myo2* mutants that are defective in binding cargoes. Moreover, fusion of Vac17 with the Myo2 CBD rescues vacuole transport in the *ptc1Δ* mutant. Altogether, these observations suggest that Ptc1 functions in the assembly of Myo2 transport complexes. Thus, Myo2 attachment to cargoes is regulated via both phosphorylation and dephosphorylation events.

A critical aspect of organelle inheritance is that only a portion or subset of the original organelles is transported to the bud while the rest is retained in the mother cell. For example, there are two distinct SPBs in each dividing cell but only one SPB is partitioned to the bud. This is essential because each SPB is attached to one complete set of chromosomes, partitioning one SPB to the bud while the other remains in the

mother cell ensures that both cells receive the proper complement of chromosomes after division. SPB partitioning is regulated via the asymmetrical loading of Kar9 onto the SPB destined for the bud and its exclusion from the mother SPB. The asymmetry of Kar9 loading ensures that Myo2 attaches to only the MTs emanating from the bud-directed SPB which is critical for the generation of a bipolar spindle. Breaking this asymmetry causes Kar9 to associate with both SPBs and the aberrant positioning of the spindle (Liakopoulos et al., 2003). Similar to SPBs, only a subset of peroxisomes is transported into the bud by Myo2. Inp2 is not uniformly localized to all peroxisomes but is enriched on the peroxisomes which are transported to the bud (Fagarasanu et al., 2009). Thus, the regulated loading of cargo adaptors contributes to the attachment of Myo2 to cargoes.

Regulation of myosin V detachment from cargoes

Accurate cargo transport requires that myosin V attaches to cargoes at their original locations and deposits cargoes at their correct destinations. Different myosin V cargoes have distinct itineraries. This strongly suggests that the detachment from myosin V is tightly regulated. Indeed, the vacuole is deposited in the bud via detachment from Myo2. A defect in this detachment causes the inappropriate transport of the bud vacuole to the mother-bud neck late in the cell cycle, the site where Myo2 delivers secretory vesicles (Karpova et al., 2000; Lillie and Brown, 1994). Detachment of the vacuole from Myo2 requires the Vac17 PEST sequence, which targets proteins for rapid turnover. Deletion of the Vac17 PEST sequence does not perturb the ability of Vac17 to bind Myo2 or Vac8 but causes an elevation of Vac17 levels. Interestingly, in

the *vac17-ΔPEST* mutant, the bud vacuole fails to detach from Myo2 and accumulates at the mother-bud neck. Thus, Vac17 degradation is required for the detachment of the vacuole from Myo2 (Tang et al., 2003).

The degradation of Vac17 involves the p21-activated kinases Cla4 and Ste20. Cla4 is a bud-specific kinase that localizes to the bud cortex and also to the vacuole upon arrival in the bud. Over-expression of either *CLA4* or *STE20* causes a decrease in Vac17 levels and a defect in vacuole transport. Interestingly, the *vac17-*Δ*PEST* mutant is not degraded even with the over-expression of *CLA4* or *STE20* (Bartholomew and Hardy, 2009). This raises the possibility that Cla4 and Ste20 phosphorylate the Vac17 PEST sequence and are part of the pathway that regulates Vac17 degradation.

The mechanisms that detach the cargoes from myosin V are likely conserved

The regulation of myosin V release of cargoes is likely conserved in most eukaryotes. Like Myo2, mammalian myosin Va, Vb and Vc move membranous organelle cargoes. Transport of these cargoes requires organelle specific adaptor proteins. For example, myosin Va transports melanosomes via interactions with melanophilin and Rab27a (Fukuda et al., 2002; Strom et al., 2002; Wu et al., 2002). Notably, melanophilin contains 3 PEST sequences, which are important for melanophilin degradation and melanosome transport (Fukuda and Itoh, 2004). The similarities between Vac17 and melanophilin, as well as the marked conservation of the cargo-binding domains of myosin V, make it tempting to speculate that the mechanisms which regulate Vac17 and the detachment of the vacuole from myosin V are similar to those that occur for other organelles throughout evolution.

In *Xenopus laevis*, myosin V CBD has been shown to play a role in the regulated detachment of cargoes. In *Xenopus* melanophores, the direct phosphorylation of myosin V regulates the release of cargoes (Rogers et al., 1999). Calcium/calmodulin-dependent protein kinase II (CaMKII) phosphorylates myosin V at Ser1650. The S1650A mutant binds but does not release melanosomes. Conversely, the S1650E phospho-mimetic mutant fails to bind to melanosomes. These observations suggest that CaMKII dependent phosphorylation of myosin V releases the melanosomes. Interestingly, myosin V is phosphorylated in the presence of mitotic but not interphase cell extracts (Karcher et al., 2001). Therefore, the phosphorylation of myosin V and the detachment of melanosomes are cell cycle regulated events. It is tempting to speculate that post-translational modification of both myosin V and its cargo adaptors regulate myosin V transport in yeast and higher eukaryotes.

Focus of the thesis

The regulated detachment of cargoes from myosin V deposits organelles at their correct subcellular locations. For the vacuole, a defect in the detachment from Myo2 causes its inappropriate transport to the mother-bud neck late in the cell cycle. Detachment of the vacuole requires the degradation of the vacuole specific adaptor for Myo2, Vac17, via its PEST sequence. Involvement of the p21 activated kinases, Cla4 and Ste20, in the degradation of Vac17, raises the possibility that post-translational modifications of Vac17 may be critical for the termination of vacuole transport. The studies described in this thesis suggest that the regulated modulation of Vac17 and the recruitment of downstream effectors directly control the detachment of the vacuole from

Myo2. Moreover, our findings suggest that the detachment of other cargoes from myosin V occurs via similar mechanisms.

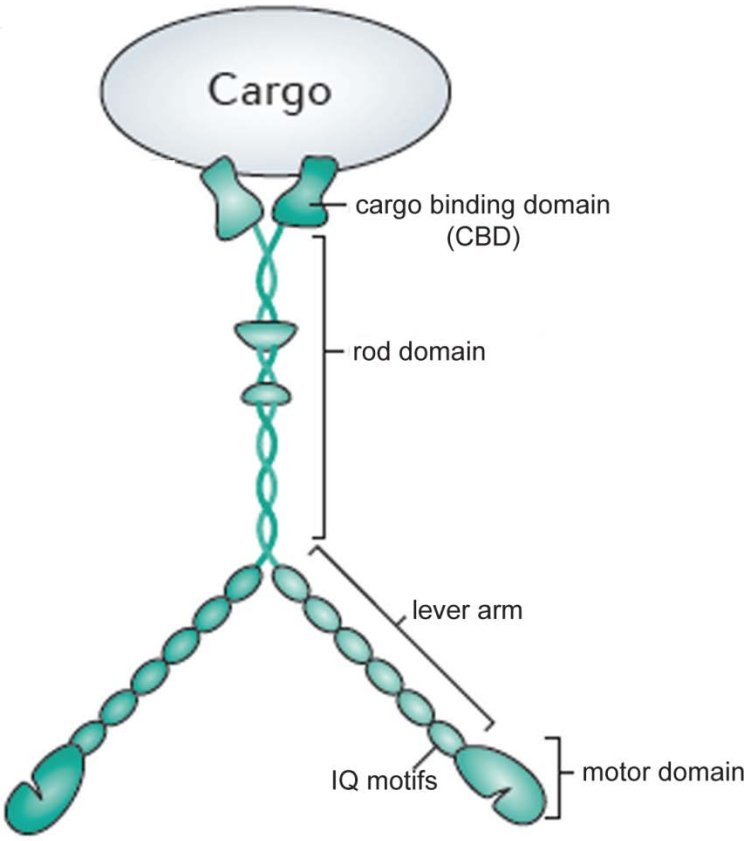

Figure 1.1. Schematic representation of myosin V.

Myosin V functions as a homodimer, each monomer consists of four main structural domains. The motor domain contains the actin and nucleotide binding site. The lever arm contains 6 IQ motifs for binding regulatory light chains. The rod domain is the site of dimerization between two myosin V heavy chains. The Cargo Binding Domain (CBD) attaches to cargoes. Image modified from (Hammer and Sellers, 2011).

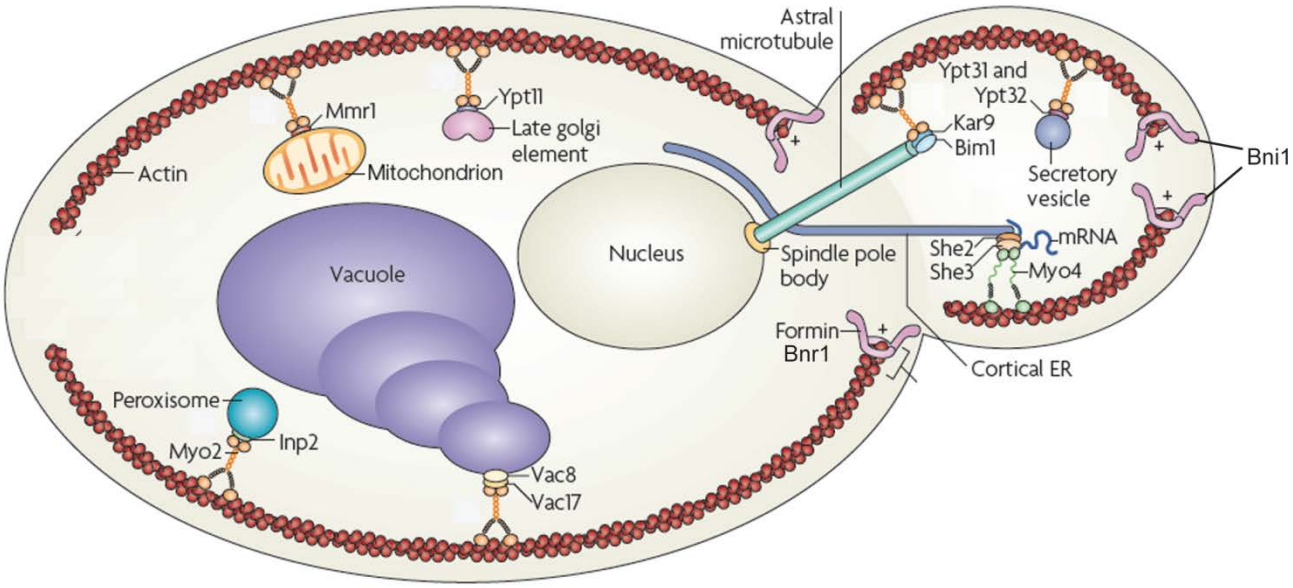

Figure 1.2. Orangelle inheritance in *S. cerevisiae*.

The formins Bnr1 and Bni1 nucleate actin cable polymerization at the bud neck and bud tip respectively. The polarity of the actin cables direct Myo2 and Myo4 transport into the bud. Myo2 attaches to different cargoes via cargo-specific adaptors. For example, Mmr1, Ypt11 (Eves et al., 2012; Fortsch et al., 2011; Itoh et al., 2004; Itoh et al., 2002), Inp2 (Fagarasanu et al., 2006), Ypt31/32, Sec4, Sec15 (Jin et al., 2011; Lipatova et al., 2008; Santiago-Tirado et al., 2011), Kar9 (Korinek et al., 2000) and Vac17 (Ishikawa et al., 2003; Tang et al., 2003) attach Myo2 to mitochondria, peroxisomes, secretory vesicles, astral microtubules and the vacuole respectively. Myo4 attaches to cER via binding She3 (Estrada et al., 2003) and attaches to mRNA via binding the She3/She2 complex (Long et al., 2000). Image modified from (Fagarasanu et al., 2010).

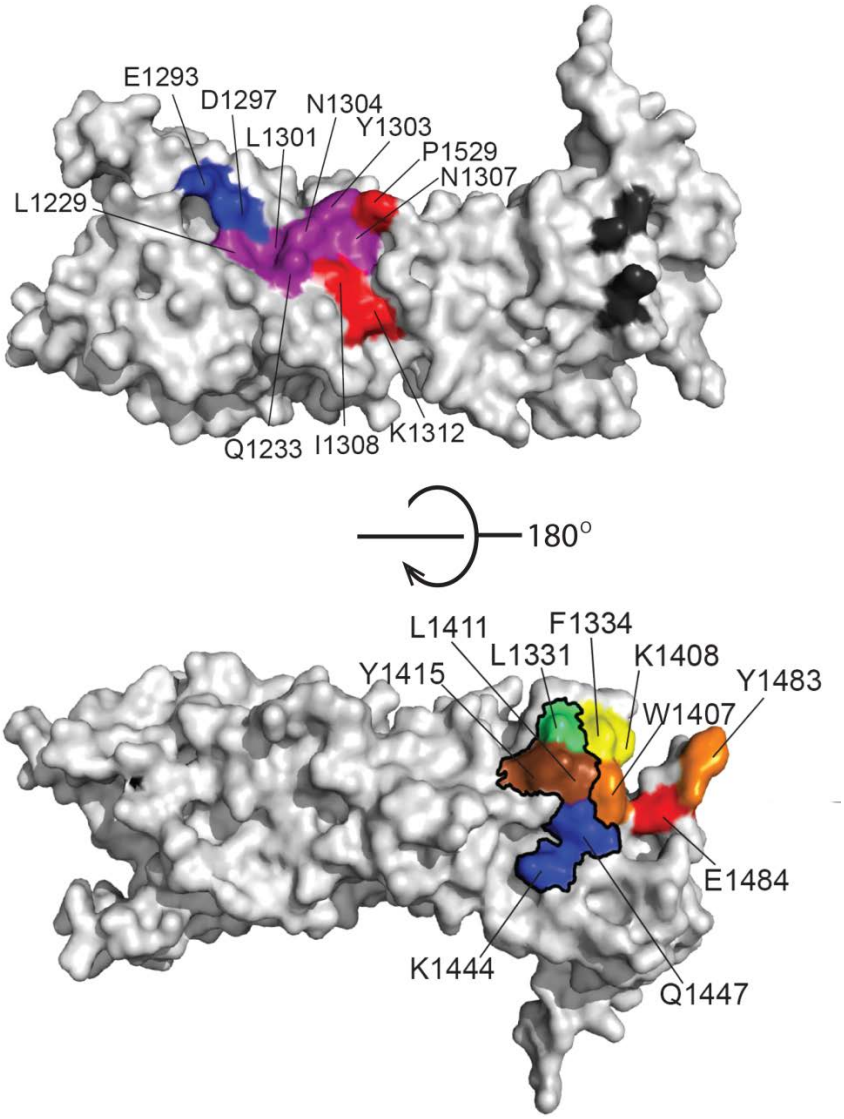

Figure 1.3. Crystal structure of the Myo2 CBD.

(Top)The Mmr1 and Vac17 binding sites partially overlap and are located in subdomain I of the Myo2 CBD. Residues E1293 and D1297 (blue) are required solely for binding Vac17. Residues I1308, K1312 and P1529 (red) are required solely for binding Mmr1. Residues L1229, L1301, N1304, Y1303 and N1307 (purple) bind both Mmr1 and Vac17. The overlap between Mmr1 and Vac17 binding sites regulate the volume of vacuole and mitochondria inherited by the bud. (Bottom) On the opposite side of the Myo2 CBD, the Ypt11, Ypt31/32, Sec4, Inp2 and Kar9 binding sites partially overlap and are located in subdomain II. F1334 and K1408 (yellow) bind Kar9. E1484 (red) binds Inp2. Y1483 and W1407 (orange) bind Kar9 and Inp2. L1331 (green) binds Kar9, Sec4 and Ypt31/32. K1444 and Q1447 (blue) bind Sec4, Ypt11 and Ypt31/32. L1411 and Y1415 (brown) bind Kar9, Inp2, Sec4, Ypt11 and Ypt31/32. Image adapted from (Eves et al., 2012).

CHAPTER II

Release from myosin V via regulated recruitment of an E3 ubiquitin ligase controls organelle localization

Introduction

Proper subcellular localization of organelles is essential for cell function. Actin based myosin V motors, conserved across eukaryotes, transport many organelles to their correct subcellular locations. Myosin V attaches to cargoes and initiates transport via the interaction of the myosin V cargo binding domain with cargo specific adaptor proteins. Upon arrival at their destinations, cargoes are released from myosin V which terminates transport and deposits cargoes at their correct subcellular locations. How molecular motors release cargoes is poorly understood.

Studies in *Saccharomyces cerevisiae* have provided significant insights into the mechanisms that regulate myosin V. The yeast myosin V motor, Myo2, transports most of the cytoplasmic organelles from the mother cell to the bud. Myo2 attaches to cargoes via direct interactions with multiple cargo specific adaptors which enable Myo2 to selectively transport subsets of cargoes to different locations at distinct times. For example, Mmr1, Ypt11(Eves et al., 2012; Fortsch et al., 2011; Itoh et al., 2004; Itoh et al., 2002), Inp2 (Fagarasanu et al., 2006), Ypt31/32, Sec4, Sec15 (Jin et al., 2011; Lipatova et al., 2008; Santiago-Tirado et al., 2011), Kar9 (Korinek et al., 2000) and Vac17 (Ishikawa et al., 2003; Tang et al., 2003) attach Myo2 to mitochondria, peroxisomes, secretory vesicles, astral microtubules and the vacuole respectively.

Studies of vacuole transport have revealed that cargo adaptors play key roles in both the spatial and temporal regulation of myosin V based transport. Early in the cell cycle, the vacuole specific adaptor, Vac17, is phosphorylated by the cyclin dependent kinase, Cdk1. Cdk1 phosphorylation promotes the interaction between Vac17 and Myo2 thereby attaching Myo2 to the vacuole (Peng and Weisman, 2008). Myo2 moves a portion of the vacuole from the mother to the bud. Initially, the vacuole in the bud remains connected to the original vacuole in the mother via a segregation structure (Weisman and Wickner, 1988). Eventually, resolution of the segregation structure separates the bud and mother vacuoles (Bartholomew and Hardy, 2009). After vacuole movement terminates, Myo2 continues to transport secretory vesicles to the mother-bud neck (Karpova et al., 2000; Lillie and Brown, 1994). Thus, Myo2 but not the bud vacuole moves to the mother-bud neck. Proper detachment of the vacuole from Myo2 requires the Vac17 PEST sequence. PEST sequences target proteins for rapid degradation. Deletion of the PEST sequence causes an accumulation of Vac17. Interestingly, in the *vac17-ΔPEST* mutant, the vacuole fails to detach from Myo2. Consequently, the vacuole is inappropriately transported to the mother-bud neck late in the cell cycle, the site where Myo2 delivers secretory vesicles (Tang et al., 2003).

Here, we present the unexpected finding that the regulated recruitment of an E3 ubiquitin ligase, Dma1, to the vacuole is critical for the accurate detachment of the vacuole from Myo2. In *S. cerevisiae*, Dma1 and its paralogue, Dma2, are known spindle positioning checkpoint proteins. In addition, they play roles in septin ring deposition, spindle positioning and cytokinesis (Fraschini et al., 2004). Dma1 and Dma2 each contain a Forkhead Associated (FHA) domain and a RING finger domain. FHA domains

bind phosphorylated threonine residues within a TxxI/L motif (Bieganowski et al., 2004; Durocher et al., 1999; Durocher et al., 2000). The RING finger domain is required for E3 ubiquitin ligase activity. Both FHA and RING domains are required for the known roles of Dma1 and Dma2 (Guertin et al., 2002; Johnson and Gould, 2011).

Here, we demonstrate that the detachment of cargoes from myosin V occurs via a novel Dma1/Dma2 dependent mechanism. For the vacuole, detachment from Myo2 requires the phosphorylation of Vac17-Thr240. This phosphorylation step occurs in the mother cell, the site where Myo2 attaches to the vacuole. Dma1 directly binds phospho-Thr240 and through this interaction, Dma1 localizes to the Myo2/Vac17 transport complex on the vacuole. Intriguingly, recruitment of Dma1 of to the vacuole is dependent on the attachment of Myo2 to the vacuole. Moreover, Dma1 is not observed on the vacuole until the vacuole enters the bud. After recruitment, Dma1 persists on the bud vacuole until after the bud vacuole separates from the mother vacuole. Subsequently, Dma1 targets Vac17 for degradation via the ubiquitin proteasome system (UPS) which releases the bud vacuole from Myo2. Thus, Vac17 phosphorylation, attachment of Myo2 to the vacuole and resolution of the segregation structure each provide different signals recognized by Dma1 which in turn detaches the vacuole from myosin V. Notably, we show that the termination of Myo2 dependent peroxisome transport also requires Dma1/Dma2. Studies on how the vacuole detaches from Myo2 will likely provide insights that are applicable to the termination of the transport of other myosin V cargoes.

Results

An E3 ubiquitin ligase, Dma1, is critical for Vac17 degradation and the termination of vacuole transport

To identify factors required for the detachment of the vacuole from Myo2, we performed a pilot genetic screen. Given that the termination of vacuole movement requires Vac17 turnover (Tang et al., 2003), we sought mutants with elevated Vac17 levels. Wild-type cells transformed with a plasmid encoding *VAC17*-GFP were subjected to EMS mutagenesis and mutants with elevated GFP fluorescence were enriched via Fluorescence Activated Cell Sorting. We obtained mutants that were defective in both the initiation and termination of vacuole transport, as both types of mutants will cause an elevation of Vac17 levels (Tang et al., 2003). Mutants defective in the initiation of vacuole transport were not pursued. One mutant of interest, *vac22-1*, had elevated levels of both Vac17-GFP and endogenous Vac17 (Figure 2.1). This indicated that the causative mutation was in a gene related to the turnover of Vac17 rather than a mutation in Vac17-GFP. In *vac22-1*, Vac17-GFP and the vacuole were mis-targeted to the mother-bud neck in large budded cells; the site where Myo2 delivers secretory vesicles late in the cell cycle (Figure 2.1). This suggests that the *vac22-1* mutant is defective in the dissociation of Vac17 and the vacuole from Myo2 causing the vacuole to be inappropriately dragged along the entire Myo2 itinerary.

To identify the causative mutation of the *vac22-1* phenotype, whole genome sequencing of the *vac22-1* genome and the isogenic parental strain genome were performed. The haploid *vac22-1* mutant was backcrossed with the isogenic wild-type strain. After 3 backcrosses, 12 spores with the *vac22-1* phenotype (elevated Vac17 levels) were pooled together and 12 spores with the wild-type phenotype (normal Vac17

levels) were pooled. Most of the potentially thousands of non-causative EMS induced mutations should randomly distribute between the mutant and wild-type pools. DNA extracted and sequenced from the mutant pool was compared to the wild-type pool (Birkeland et al., 2010). The point mutation, *dma1-G232R*, was present only in the mutant pool and absent from the wild-type pool.

To determine if *DMA1* is required for the termination of vacuole movement, we generated a *dma1Δ* mutant. We assessed the location of the vacuole in large budded cells, where Myo2 is predicted to localize to the mother-bud neck. In the *dma1Δ* mutant, 40.0±0.5% of large budded cells have vacuoles mis-targeted to the mother-bud neck. That the inappropriate accumulation of vacuoles at the mother-bud neck did not exceed 40% is likely due to the fact that in a percentage of large budded cells the actin cytoskeleton has yet to be re-organized and Myo2 has not yet moved to the mother-bud neck (Pruyne et al., 2004b). The presence of vacuoles at the mother-bud neck of wild-type cells was much lower, approximately 10% of large budded cells have this phenotype (Figure 2.2). Furthermore, in the *dma1Δ* mutant, the vacuole colocalized with Vac17-GFP and Myo2-Venus at the mother-bud neck (Figure 2.3). These results suggest that Dma1 is required for the detachment of Vac17 and the vacuole from Myo2.

Expression of *DMA1* but not *dma1-G232R* restores the termination of vacuole movement in the *dma1Δ* mutant (Figure 2.2) and in the *vac22-1* mutant (data not shown). Furthermore, expression of *DMA1* but not *dma1-G232R* rescued Vac17 levels in the *dma1Δ* mutant (Figure 2.2) and in the *vac22-1* mutant (data not shown). Therefore, *dma1-G232R* is the causative mutation of the *vac22-1* phenotype.

Dma2, the paralogue of Dma1 in *S. cerevisiae*, shares 58% amino acid identity

with Dma1 and performs redundant functions in the spindle positioning checkpoint and cytokinesis (Fraschini et al., 2004). To test whether Dma2 also functions in the termination of vacuole movement, the *dma2Δ* and *dma1Δ dma2Δ* mutants were generated. In the *dma2Δ* mutant, there was a modest phenotype, 17.3±3.67% of large budded cells accumulate vacuoles at the mother bud neck compared to the *dma1Δ* mutant at 41.6±3.32%. In the *dma1Δ dma2Δ* double mutant the phenotype was stronger (71.9±5.90%). In wild-type cells, only 10.5±1.04% of large budded cells show this phenotype (Figure 2.4). These results suggest that Dma2 also functions in the termination of vacuole movement.

We tested whether Dma1 and Dma2 are required for the termination of the transport of peroxisomes, another Myo2 cargo. We chose peroxisomes because their transport is entirely Myo2 dependent and similar to the vacuole, the peroxisome remains intact after transport (Fagarasanu et al., 2006). To visualize peroxisomes, we tagged GFP with the peroxisome targeting sequence, SKL. In wild type cells, peroxisomes are distributed along the periphery of the bud with only 2.1±1.4% of large budded cells showing accumulation of peroxisomes at the mother-bud neck. In the *dma1Δdma2Δ* mutant, peroxisomes were mis-targeted to the mother-bud neck in 56.1±2.2% of large budded cells. This phenotype closely parallels the accumulation of vacuoles at the mother-bud neck in the *dma1Δdma2Δ* mutant (Figure 2.5). These results suggest Dma1 and Dma2 function with Myo2 to release at least two types of cargoes. Thus, mechanistic insights gained from studies of Dma1/Dma2 are likely to be applicable to other myosin V cargoes. To further investigate the mechanisms by which Dma1 and Dma2 regulate cargo release, we focused on the vacuole.

Dma1 localizes to the bud vacuole

Dma1 functions as a spindle checkpoint protein in *Schizosaccharomyces pombe* (Murone and Simanis, 1996). In *S. pombe*, Dma1 localizes to the cytokinetic ring and the spindle pole bodies (SPBs), however, its localization in *S. cerevisiae* was unknown (Guertin et al., 2002). We found that in *S. cerevisiae*, Dma1-GFP localized to regions consistent with the septin ring and the SPBs and colocalized with Spc42-mRFP (Figure 2.6), a core component of the SPB. Dma1 localizes to the SPBs and septin ring only in large budded cells late in the cell cycle. That Dma1 functions in the termination of vacuole transport prompted us to examine the localization of Dma1 during vacuole inheritance. Early in the cell cycle, we found that Dma1-GFP localized to the vacuole in the bud and did not colocalize with Spc42-mRFP, which remained in the mother cell (Figure 2.6).

To further determine the timing of Dma1 localization to the vacuole, *DMA1* was tagged with 3xGFP at its endogenous locus. Dma1-3xGFP localization was assessed during vacuole inheritance, from prior to the initiation of vacuole transport until the resolution of the segregation structure. In unbudded and small budded cells where the vacuole has not moved into the bud, no significant localization of Dma1-3xGFP to the vacuole was observed. Dma1-3xGFP was first observed on the portion of the vacuole that crossed the mother-bud neck into the bud. At this time, the vacuole in the bud is connected to the mother vacuole via a segregation structure. Intriguingly, after Dma1 was recruited to the vacuole, the termination of vacuole transport did not immediately occur. Instead, Dma1-3xGFP moved with the vacuole to the bud tip and remained on the vacuole as the bud grew. Dma1-3xGFP persisted on the vacuole at the bud tip until

after the segregation structure was resolved and the bud vacuole separated from the mother vacuole (Figure 2.7). These results suggest that both recruitment of Dma1 to the vacuole and Dma1 activity are coordinated with vacuole inheritance.

To determine whether recruitment of Dma1 to the vacuole is dependent on Myo2, we tested a condition where Myo2 does not attach to the vacuole and analyzed Dma1-GFP localization in a *myo2-D1297N* mutant. The *myo2-D1297N* mutant does not bind Vac17 and the vacuole is not transported to the bud (Eves et al., 2012; Ishikawa et al., 2003). We found that Dma1-GFP failed to accumulate on the vacuole in the *myo2-D1297N* mutant in all small budded cells analyzed. In contrast, in cells expressing *MYO2,* Dma1-GFP accumulated on the bud vacuole in 76.4±5.7% of small budded cells (Figure 2.8). These results suggest that Dma1 recruitment to the vacuole requires the assembly of the Myo2/Vac17/Vac8 complex. Interestingly, in the *myo2-D1297N* mutant, where Dma1 is not recruited to the vacuole, Vac17 is not degraded (Figure 2.8). This suggests that the regulated recruitment of Dma1 to the vacuole is critical for Vac17 degradation.

Vac17 residues Ser222 and Thr240 are required for Vac17 degradation and the termination of vacuole transport

The Vac17 PEST sequence is required for the termination of vacuole transport (Tang et al., 2003) (Figure 2.9). PEST sequences contain serines and threonines that are often phosphorylation sites critical for targeting the protein for degradation (Marchal et al., 1998; Martinez et al., 2003). We performed an alanine scan of the threonines and serines within the Vac17 PEST sequence to identify potential phosphorylation sites

required for Vac17 degradation. Two point mutants, *vac17-S222A* and *vac17-T240A*, caused an elevation in Vac17 levels (Figure 2.9).

To determine whether these point mutations cause a defect in the termination of vacuole transport, both *vac17* point mutants were tagged with GFP. In large budded cells expressing *VAC17*-GFP, no GFP signal was detected and the vacuole remained in the bud suggesting that Vac17-GFP was properly degraded and that the vacuole has detached from Myo2. In contrast, *vac17-S222A*-GFP and *vac17-T240A*-GFP as well as the vacuole accumulated at the mother-bud neck in large budded cells. In cells expressing *vac17-S222A* or *vac17-T240A*, but not *VAC17*, the vacuole colocalized with Myo2-Venus at the mother-bud neck. Moreover, *vac17-S222A*-GFP and *vac17-T240A*-GFP colocalized with mCherry-Myo2 at the mother-bud neck. The lack of a GFP signal in cells expressing *VAC17*-GFP suggests that Vac17 has already been degraded (Figure 2.10). Together, these results suggest that Vac17 residues Ser222 and Thr240 are required for Vac17 degradation and the regulated detachment of Vac17 and the vacuole from Myo2.

Dma1 binds directly to Vac17 at phosphorylated Thr240 *in vitro*

Vac17-Thr240 is found within the sequence $T_{240}IIL_{243}$, which matches the TxxI/L motif recognized by FHA domains. Therefore, Vac17-Thr240 may serve as the binding site for Dma1. Because FHA domains bind phosphorylated threonines, we hypothesized that Thr240 is phosphorylated.

To determine whether Thr240 is a phosphorylation site *in vivo*, we generated antibodies against a peptide with a central phosphorylated Thr240. To analyze Vac17

phosphorylation, we immunoprecipitated Vac17-GFP expressed in a *vac17*Δ mutant using anti-GFP antibodies. However, we failed to detect Vac17-GFP via western blot or immunoprecipitation (IP) (Figure 2.11). In wild-type cells, Vac17 levels are exceedingly low, present at ~20 molecules per cell (Ghaemmaghami et al., 2003; Tang et al., 2006). Thus, detecting phosphorylated Vac17 proved difficult. However, we postulated that Dma1 and Dma2 targets Vac17 for degradation by binding phosphorylated Thr240. Deletion of *DMA1* and *DMA2* would likely result in the accumulation of phosphorylated forms of Vac17 (Figure 2.11). Indeed, Vac17-GFP levels were elevated when expressed in the *dma1Δ dma2Δ vac17Δ* mutant. Moreover, Vac17-GFP was recognized by the anti- phospho-Thr240 antibody. In contrast, the levels of *vac17-T240A*-GFP are similar when expressed in both the *vac17Δ* and *dma1Δ dma2Δ vac17Δ* mutants, but was not recognized by the anti-phospho-Thr240 antibody, verifying the specificity of this antibody for Thr240.

To further determine whether this antibody is phospho-specific, Vac17-GFP was expressed and immunoprecipitated from the *dma1Δ dma2Δ vac17Δ* mutant and treated with λ-phosphatase. Vac17-GFP was dephosphorylated, as indicated by an increase in its electrophoretic mobility, in samples treated with λ-phosphatase but not with the addition of phosphatase inhibitors or in untreated samples (Figure 2.11). Importantly, the anti-phospho-Thr240 antibody failed to recognize phosphatase treated Vac17-GFP indicating that this antibody is specific for phosphorylated Thr240 and that Thr240 is phosphorylated *in vivo*. These results strongly suggest that Vac17-Thr240 is a binding site for Dma1. Moreover, given that *vac17-T240A-GFP* levels were similar in the absence and presence of *DMA1/DMA2* suggests that Thr240 and Dma1/Dma2 function

in the same step of the pathway.

To test whether Dma1 binds phosphorylated Vac17-Thr240, *in vitro* binding studies were performed. Recombinant GST-Dma1 or the GST tag alone were immobilized on glutathione beads and incubated with yeast cell extracts from a *dma1*Δ *dma2*Δ *VAC17-TAP* strain where Vac17 levels are elevated and Vac17 is phosphorylated. GST-Dma1 but not the GST tag alone bound Vac17-TAP. However, GST-Dma1 did not bind *vac17-T240A*-TAP. As a control, we show that the Myo2 cargo binding domain, a known Vac17 binding partner, bound the *vac17-T240A*-TAP mutant (Figure 2.12). This suggests that the T240A mutation does not affect the overall structure of Vac17 and that Thr240 is required for Dma1 to bind Vac17.

To further test whether Dma1 binds directly to phosphorylated Thr240, competition experiments were performed. Prior to incubation with yeast cell extracts, immobilized GST-Dma1 was first incubated with peptides that contained either a central phosphorylated Thr240, unphosphorylated Thr240 or phosphorylated Ser222. The phosphorylated Thr240 peptide blocked GST-Dma1 from binding Vac17-TAP from cell lysates. The unphosphorylated Thr240 or phosphorylated Ser222 peptides, did not affect GST-Dma1 binding to Vac17-TAP (Figure 2.13). Thus, Dma1 binds directly to Vac17 at phosphorylated Thr240. Furthermore, these results suggest that Dma1 does not bind Vac17-Ser222. Consistent with this hypothesis, we found that recombinant GST-Dma1 bound *vac17-S222A*-TAP *in vitro* (Figure 2.14).

Recruitment of Dma1 to the vacuole requires the interaction between Dma1 and phosphorylated Vac17-Thr240

To test whether Vac17-Thr240 is required for the recruitment of Dma1 to the vacuole, we analyzed the localization of Dma1-GFP in cells expressing *VAC17* or *vac17-T240A*. In cells expressing *VAC17*, Dma1-GFP localized to the vacuole in 82.9±4.3% of small budded cells. In contrast, Dma1-GFP localization to the vacuole occurred in 19.5±1.9% of small budded cells expressing *vac17-T240A*. Similarly, Dma1-tdTomato colocalized with Vac17-GFP in 79.8±2.4% of small budded cells and with *vac17-T240A*-GFP in 33.6±5.3% of small budded cells (Figure 2.15).

Given that FHA domains bind phosphorylated threonine within a TxxI/L motif, we tested whether the FHA domain of Dma1 is required for Dma1 recruitment to Vac17. We generated the *dma1-R193E* mutant, which contains a charge reversal of a conserved residue in FHA domains that directly contacts phospho-threonine (Durocher et al., 2000). While Dma1-GFP localized to the vacuole in 75.4±4.4% of small budded cells, *dma1-R193E*-GFP failed to localize to the vacuole in all cells analyzed (Figure 2.16). These results suggest that interaction between the Dma1 FHA domain and phosphorylated Vac17-Thr240 is critical to recruit Dma1 to the vacuole.

Dma1 is first observed on the vacuole in the bud. Furthermore, Dma1 is not recruited to the mother vacuole in the *myo2-D1297N* mutant. These observations raise the question of whether phosphorylation of Vac17-Thr240 is bud-specific. Surprisingly, we found that in the *myo2-D1297N* mutant, where Vac17-GFP is localized to the mother vacuole, Vac17-Thr240 was phosphorylated (Figure 2.17). We compared the phosphorylation of Vac17-Thr240 in the *myo2-D1297N* mutant with the phosphorylation of the *vac17-S222A* mutant. The S222A point mutation stabilizes Vac17, enables vacuole transport and accumulates in the bud (Figure 2.17). Vac17-GFP in the *myo2-*

D1297N mutant and *vac17-S222A*-GFP are phosphorylated at Thr240 to similar extents. As expected, the *vac17-T240A*-GFP mutant was not phosphorylated at Thr240. These results suggest that Thr240 is phosphorylated in the mother cell. Moreover, phosphorylation of Vac17 does not require Myo2. These observations strongly suggest that that Vac17 is phosphorylated on Thr240 in the mother cell prior to the attachment of Myo2 to the vacuole and the initiation of vacuole transport. The failure of Dma1 recruitment to the mother vacuole in the *myo2-D1297N* mutant is not due to a defect in the phosphorylation of Vac17-Thr240. Thus, phosphorylation of Vac17-Thr240 is required but not sufficient for recruiting Dma1 to the vacuole.

Interestingly, in cells expressing *vac17-S222A*, another mutant that causes a defect in the termination of vacuole transport, Dma1-GFP localized to the vacuole in 79.4±2.6% of small budded cells. Further, Dma1-tdTomato colocalized with *vac17-S222A*-GFP in the bud in 87.5±4.5% of small budded cells (Figure 2.15). Thus, Ser222 is not required for the recruitment of Dma1 to the vacuole transport complex. Furthermore, Dma1 binds *vac17-S222A in vitro* (Figure 2.14). Together, these results suggest that after Dma1 is recruited to the vacuole, Ser222 functions in downstream events that are required for the detachment of the vacuole from Myo2.

Dma1/Dma2 function in the ubiquitylation of Vac17

In *S. pombe*, the E3 ubiquitin ligase activity of Dma1 is required for its function as a spindle checkpoint. *S. Pombe* Dma1-Ile194 is a conserved residue in the RING domain that is required for Dma1 dependent ubiquitylation *in vitro* and for Dma1 spindle checkpoint function *in vivo* (Johnson and Gould, 2011). This conserved isoleucine is

critical for the interaction between E3 ubiquitin ligases with their E2 ubiquitin conjugating enzyme binding partners (Zheng et al., 2000). To determine whether the E3 ubiquitin ligase activity of *S. cerevisiae* Dma1 is required for the termination of vacuole transport, we mutated the Dma1-I329 residue which is homologous with *S. pombe* Dma1-I194.

We found that in contrast to Dma1 and Dma1-GFP, the ubiquitylation-defective mutant, *dma1-I329*-GFP, failed to target Vac17 for degradation (Figure 2.18) or rescue the termination of vacuole transport in the *dma1Δ* mutant (Figure 2.19). Moreover, the vacuole accumulates with Vac17-GFP and Myo2-Venus at the mother-bud neck in large budded cells in the *dma1-I329R* mutant (Figure 2.20). Thus, Dma1 dependent ubiquitylation is required for Vac17 degradation and the detachment of the vacuole from Myo2.

To test whether the I329R mutation disrupts Dma1 binding to Vac17, *in vitro* binding experiments were performed. GST-*dma1-I329R* bound Vac17-TAP from cell extracts (Figure 2.21). These results suggest that the E3 ubiquitin ligase activity of Dma1 is not required for Dma1 to bind Vac17.

We found that the levels of the ubiquitylation defective mutant *dma1-I329R*-GFP are higher than wild-type levels (Figure 2.18). Wild-type Dma1 auto-ubiquitylates *in vitro* (Loring et al., 2008), which predicts that the *dma1-I329R* mutant is defective in the regulation of its own turnover. Given that Vac17 recruits Dma1 to the vacuole and that both Vac17 and *dma1-I329R* levels are elevated (Figure 2.18) may explain why *dma1-I329R*-GFP localizes to a broader area on the bud vacuole (Figure 2.22).

The requirement for the E3 ligase activity of Dma1 for Vac17 degradation suggests that Vac17 is ubiquitylated. To test this hypothesis, we immunoprecipitated

Vac17-GFP using anti-GFP antibodies from cells which express myc tagged ubiquitin (myc-Ub). Immunoblot analysis using anti-myc antibodies showed that Vac17-GFP was ubiquitylated *in vivo*. However, in the absence of *DMA1*/*DMA2*, Vac17-GFP levels were elevated but not detectably ubiquitylated (Figure 2.23). These results strongly suggest that Dma1 and Dma2 are required for Vac17 ubiquitylation *in vivo*.

That Vac17 is ubiquitylated suggests that the ubiquitin proteasome system (UPS) is important for Vac17 degradation. We found that Vac17 levels were elevated in the E1 mutant, *uba1-2*, as well as in the proteasome mutants tested, *pre1-1*, *doa2-T76A* and *pup1-K58E*/*pup3-E151K* (Figure 2.24). These results suggest that Dma1 ubiquitylates Vac17 and targets Vac17 for degradation via the proteasome.

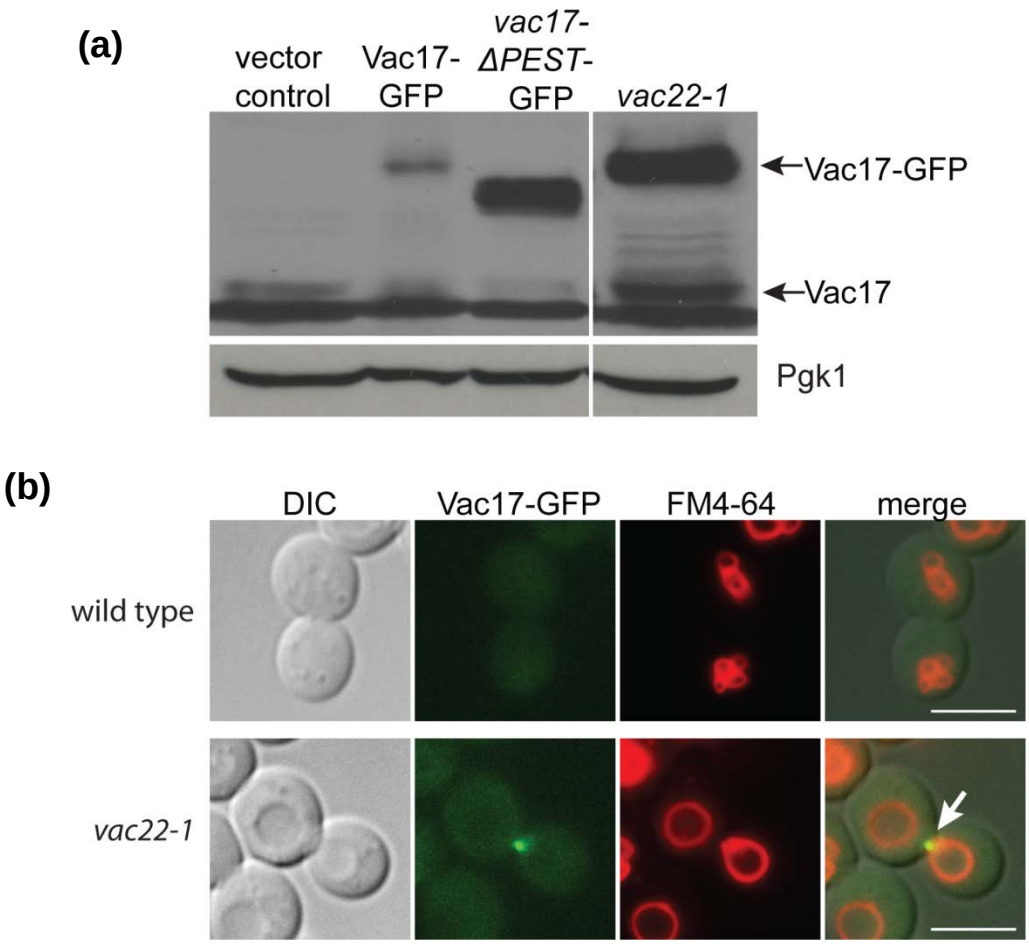

Figure 2.1. *vac22-1* is defective in the termination of vacuole transport.

Wild-type cells transformed with a Vac17-GFP plasmid was subjected to EMS mutagenesis. Fluorescence Activated Cell sorting (FACS) isolated mutants with elevated GFP fluorescence. (a) The *vac22-1* mutant, has elevated levels of both Vac17-GFP and endogenous Vac17. anti-Vac17 antibodies; 1:1,000 dilution. anti-Pgk1antibodies (input control); 1:10,000 dilution. (b) Vac17-GFP and the vacuole are inappropriately transported to the mother-bud neck in the *vac22-1* mutant (arrow). This suggests that the defect in the *vac22-1* mutant is in the detachment of Vac17 and the vacuole from Myo2. Bar = 5 μm. (Screen and initial characterization were performed by Yutian Peng. Western blot and initial characterization of *vac22-1* by microscopy performed by Rajeshwari Valiathan. Images shown in (b) were obtained by Richard Yau).

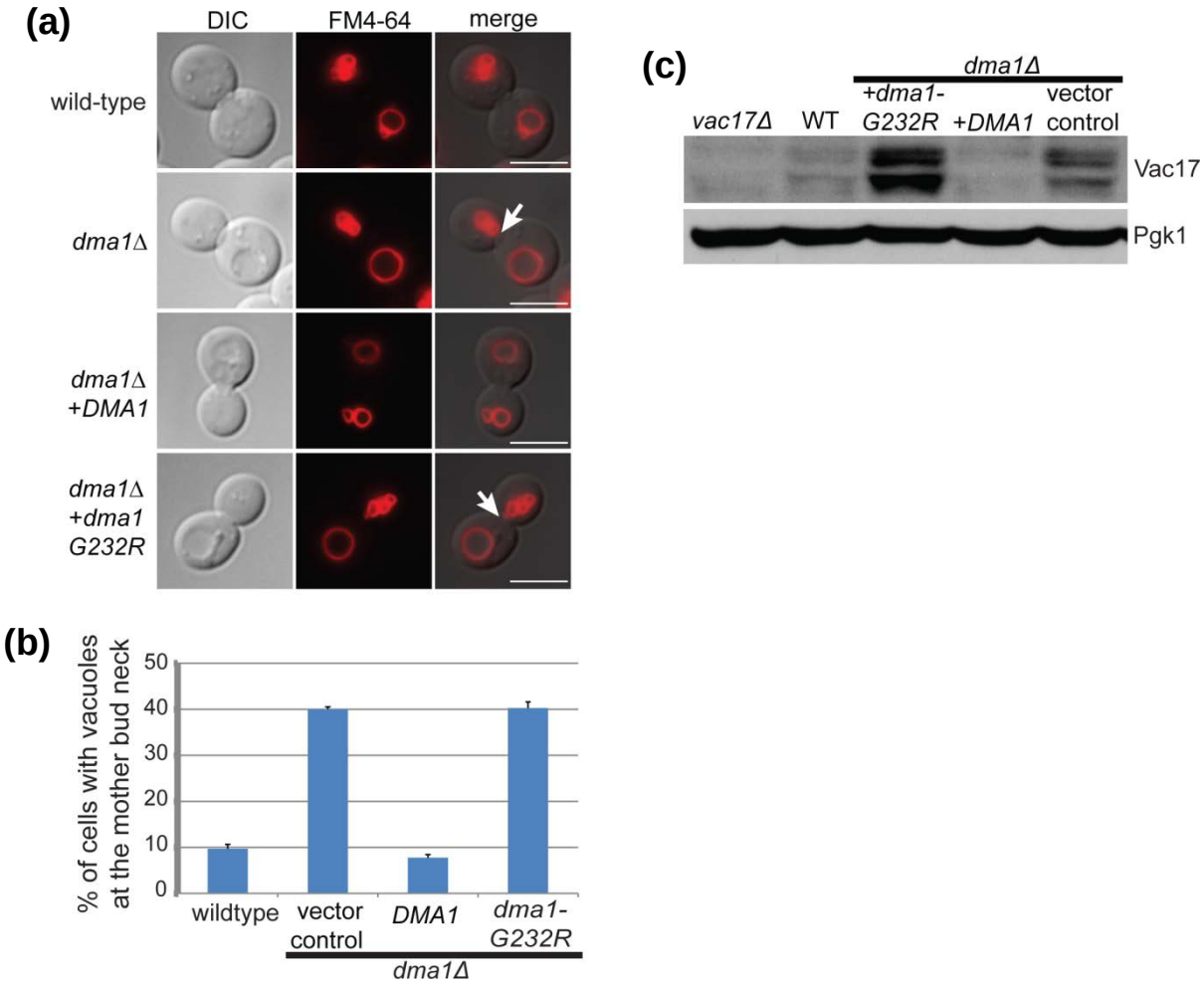

Figure 2.2. *dma1-G232R* is defective in the termination of vacuole transport.

DMA1 was deleted from the wild-type strain genome, vacuole transport was assessed via FM4-64 labeling and Vac17 levels were tested via western blot. (a) The vacuole accumulates at the mother-bud neck in the *dma1Δ* mutant, expression of *DMA1* but not *dma1-G232R* restores the proper position of the vacuole in the bud. Arrows; accumulation of Vac17 and vacuoles at the mother-bud neck. (b) Percentage of large budded cells with the accumulation of vacuoles at the mother-bud neck in the absence of *DMA1*. Expression of *DMA1* but not *dma1-G232R* restores the proper position of the bud vacuole in the *dma1Δ* mutant. A minimum of 100 cells were counted per experiment for 3 experiments. Error bars; standard error of the mean (SEM). Bar = 5 μm. (c) Vac17 levels are elevated in the *dma1Δ* mutant, expression of *DMA1* but not *dma1-G232R* rescues Vac17 levels. anti-Vac17 antibodies; 1:1,000 dilution. anti-Pgk1 antibodies (input control); 1:10,000 dilution.

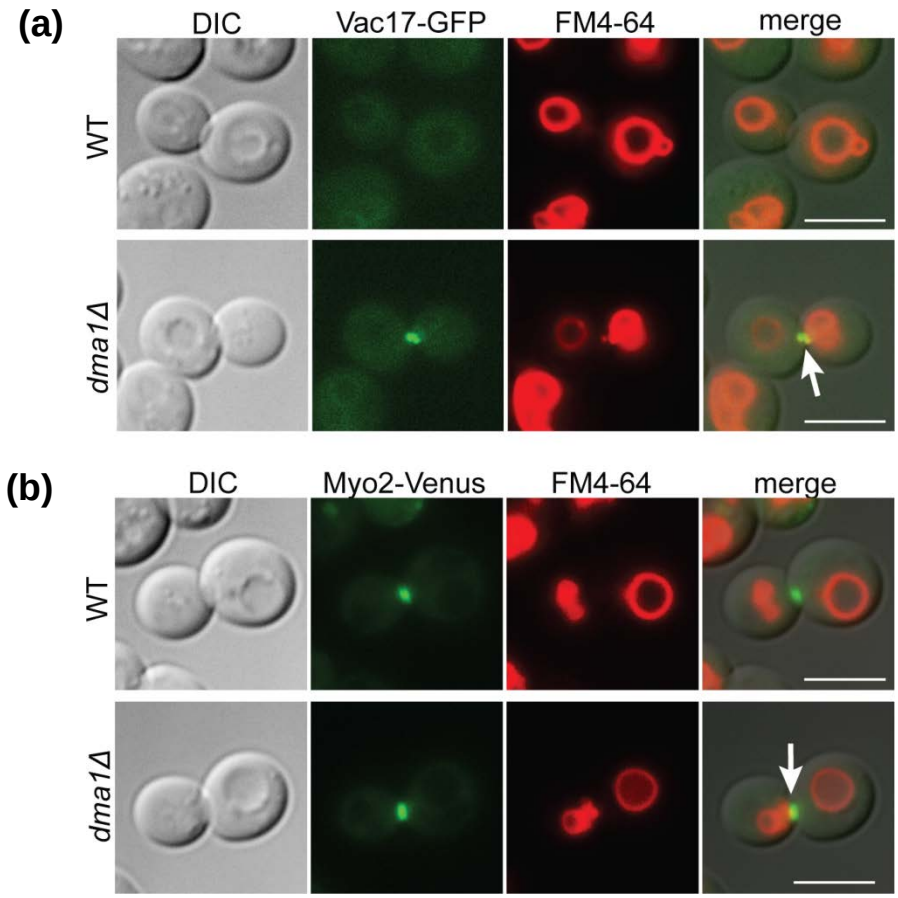

Figure 2.3. *DMA1* is required for the detachment of Vac17 and the vacuole from Myo2.

In a *dma1*Δ mutant, Vac17-GFP and vacuoles are mis-targeted to the mother-bud neck (a) and vacuoles colocalize with Myo2-Venus at the mother-bud neck (b). In the absence of *DMA1*, the continued association of Vac17 with Myo2 causes the inappropriate transport of the vacuole to the mother-bud neck, the site where Myo2 delivers secretory vesicles late in the cell cycle. Bar = 5 μm.

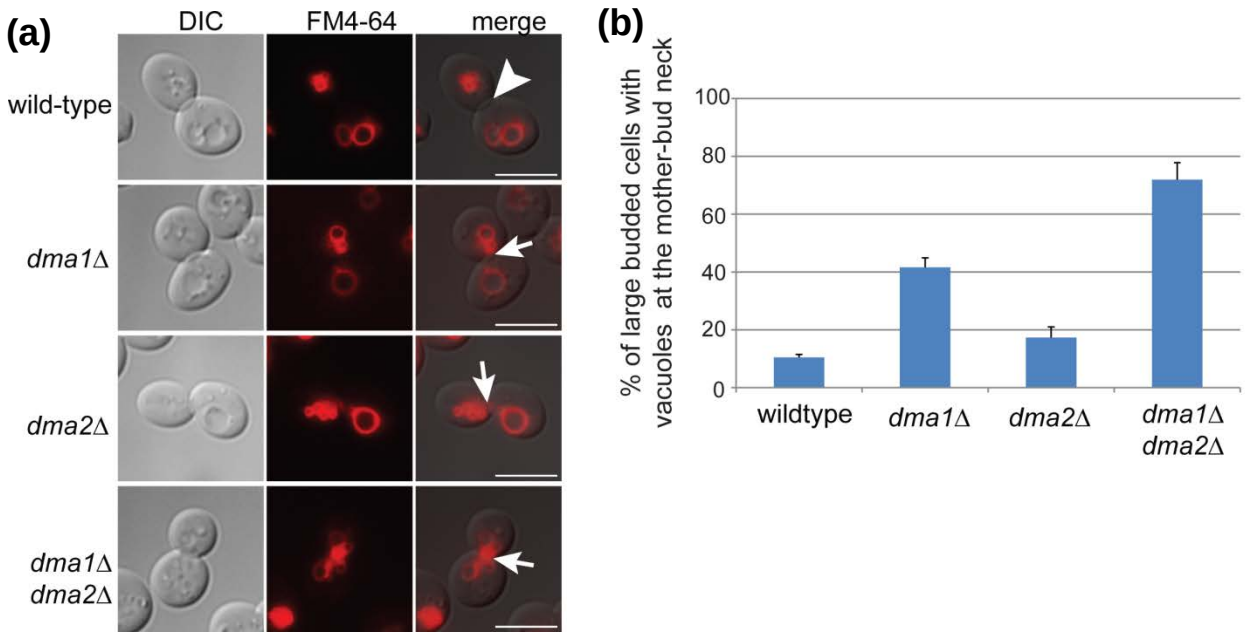

Figure 2.4. *DMA2* functions in the termination of vacuole transport.

(Left) In the *dma1Δ*, *dma2Δ* and double *dma1Δ dma2Δ* mutants, termination of vacuole transport is defective (arrows). (Right) Percentage of large budded cells with vacuoles accumulated at the mother-bud neck in the mutants shown in (a). A minimum of 129 cells were counted per experiment for 3 experiments. Error bars; SEM. Bar = 5 μm.

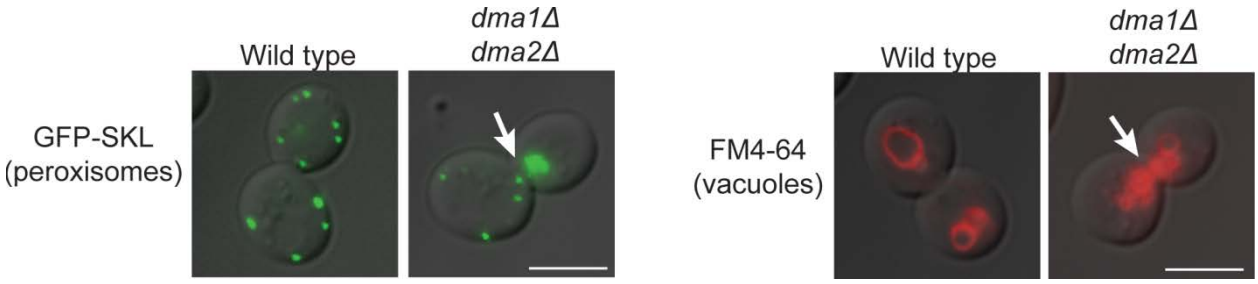

Figure 2.5. The termination of peroxisome transport requires *DMA1/DMA2*.

To visualize peroxisomes, GFP was tagged with the peroxisome targeting sequence, SKL, and expressed from a plasmid. In a *dma1*Δ*dma2*Δ double mutant. (Left) Peroxisomes accumulate at the mother-bud neck late in the cell cycle (arrow). (Right) Vacuoles also accumulate at the mother-bud neck in this mutant (arrow). This suggests that the mechanisms which terminate vacuole transport are similar to those which terminate peroxisome transport. Bar = 5 μm.

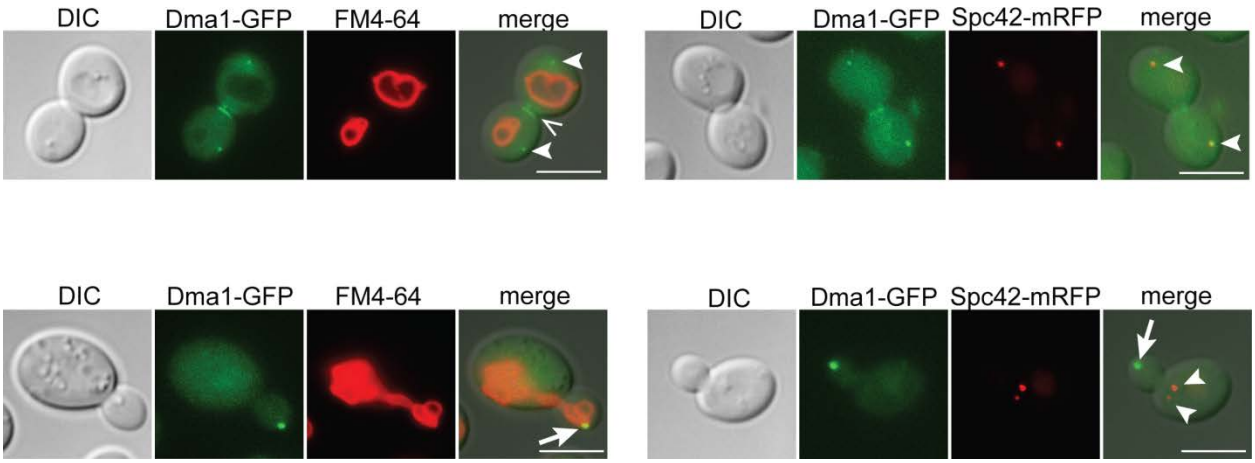

Figure 2.6. Dma1 localizes to the SPBs, cytokinetic ring and the vacuole.

(Top-left) In large budded cells, Dma1-GFP localizes to regions consistent with the SPBs (arrowhead) and septin ring (<). (Top-right) Dma1-GFP colocalizes with Spc42-mRFP, a component of the SPB (arrow heads). (Bottom-left) In small budded cells, Dma1-GFP localizes to the vacuole in the bud (arrow). (Bottom-right) Dma1-GFP does not colocalize with Spc42-mRFP (arrow heads). Bar = 5 μm.

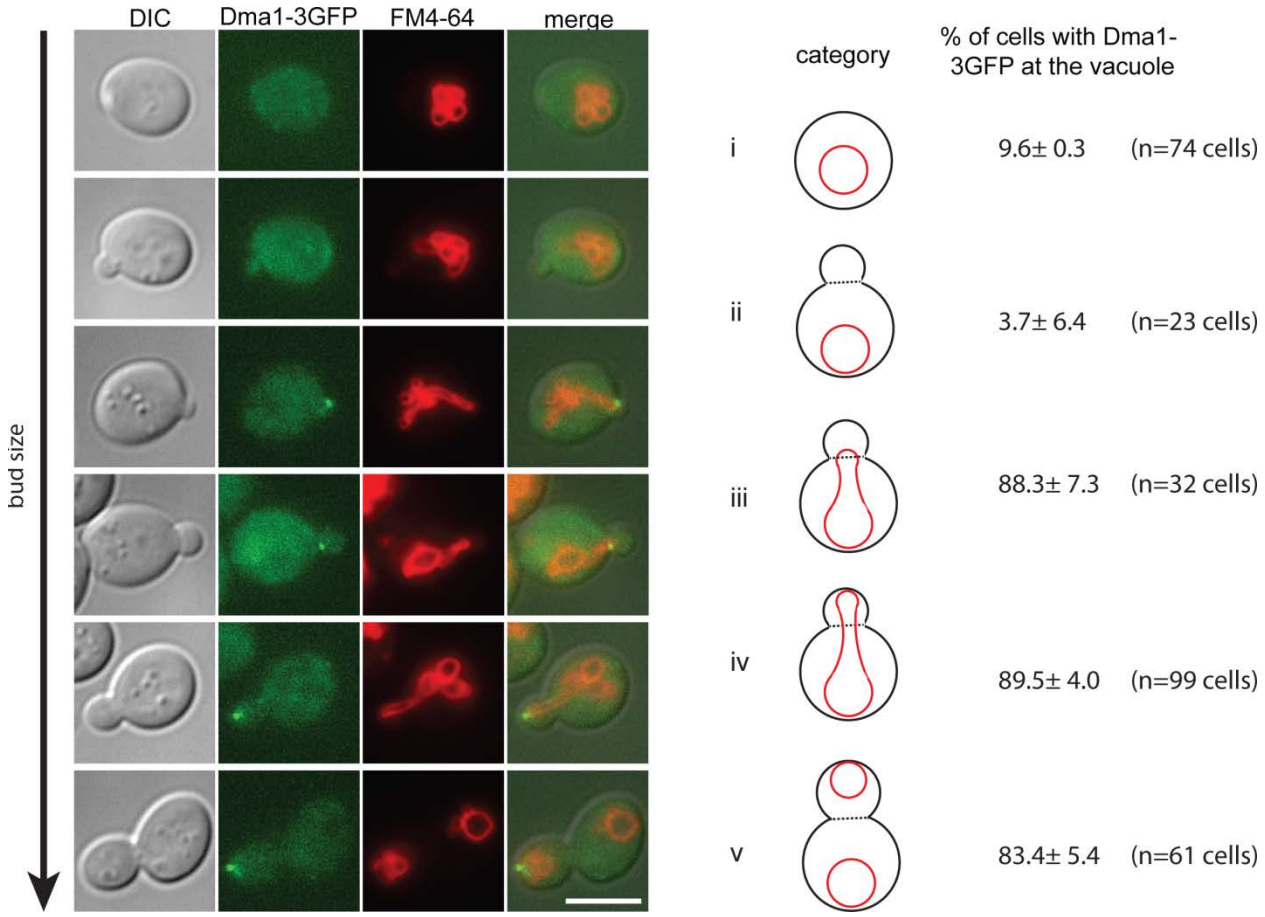

Figure 2.7. Dma1 localizes to the vacuole during transport.

(Left) Dma1-3xGFP, expressed from its endogenous locus, is first observed on the vacuole as the vacuole crosses the mother-bud neck. The vacuole continues to move to the bud tip and Dma1 remains on the vacuole until after the resolution of the segregation structure. (Right) Percentage of cells with Dma1 at the vacuole in (i) unbudded cells, (ii) small budded cells where the vacuole is in the mother, (iii) small budded cells where the vacuole has crossed the mother-bud neck, (iv) small budded cells where the vacuole has reached the bud tip, (v) medium budded cells where the segregation structure was resolved. Z-sections of small budded cells were analyzed. A minimum of 25 cells were counted per experiment for 3 experiments. Error bars; standard error of the mean (SEM). Bar = 5 μm

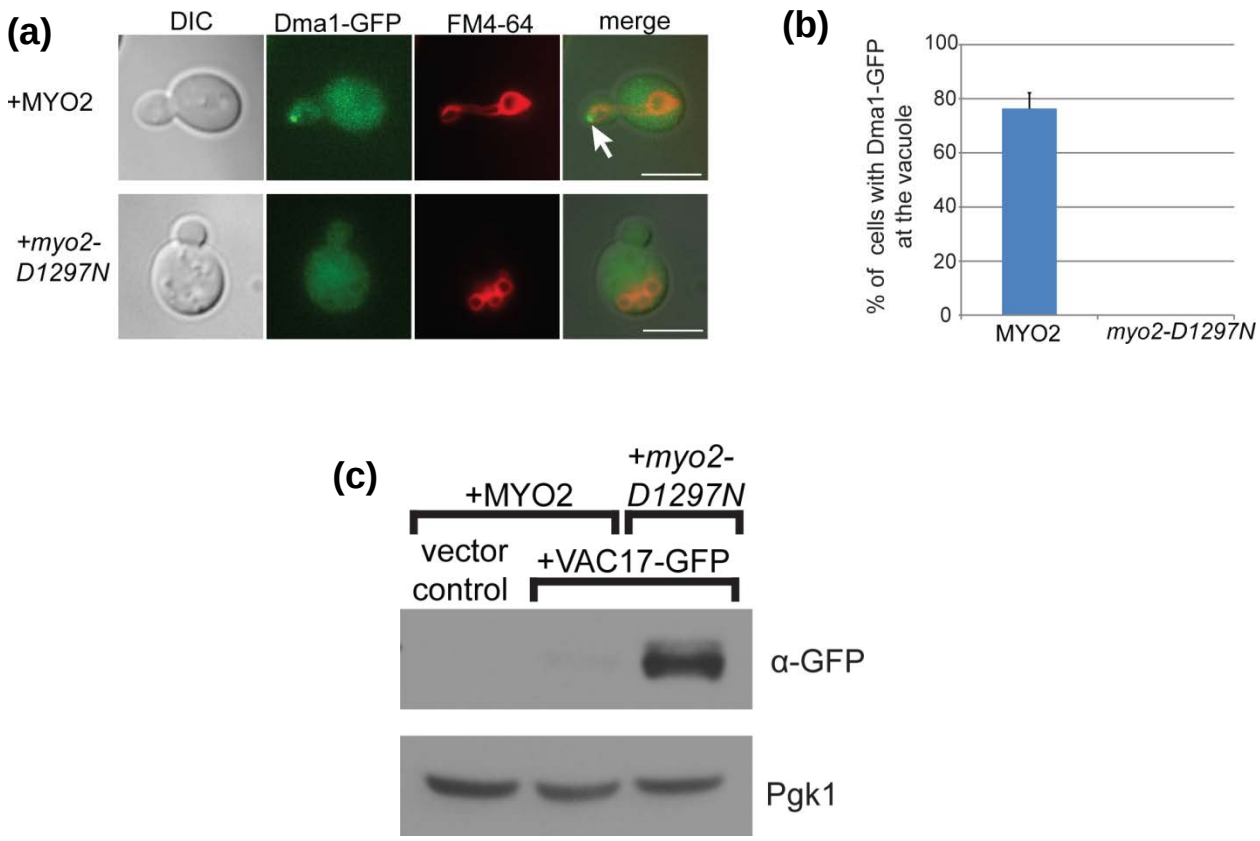

Figure 2.8. Recruitment of Dma1 to the vacuole requires assembly of the vacuole transport complex.

The *myo2Δdma1Δ* double mutant was co-transformed with *DMA1*-GFP and *MYO2* or *myo2-D1297N* plasmids. (a) Dma1-GFP localizes to the vacuole in the bud in cells expressing *MYO2*, but fails to localize to the mother vacuole in cells expressing *myo2-D1297N*, a mutant defective in vacuole transport. Bar = 5 μm. (b) Quantification of the percentage of small budded cells where Dma1-GFP localizes to the vacuole. Z-sections of small budded cells were analyzed. A minimum of 25 cells were counted per experiment for 3 experiments. Error bars; standard error of the mean (SEM). (c) In the *myo2-D1297N* mutant, Vac17-GFP levels are elevated compared to cells expressing *MYO2*. anti-GFP; 1:1,000 dilution. anti-Pgk1 antibodies; 1:10,000 dilution.

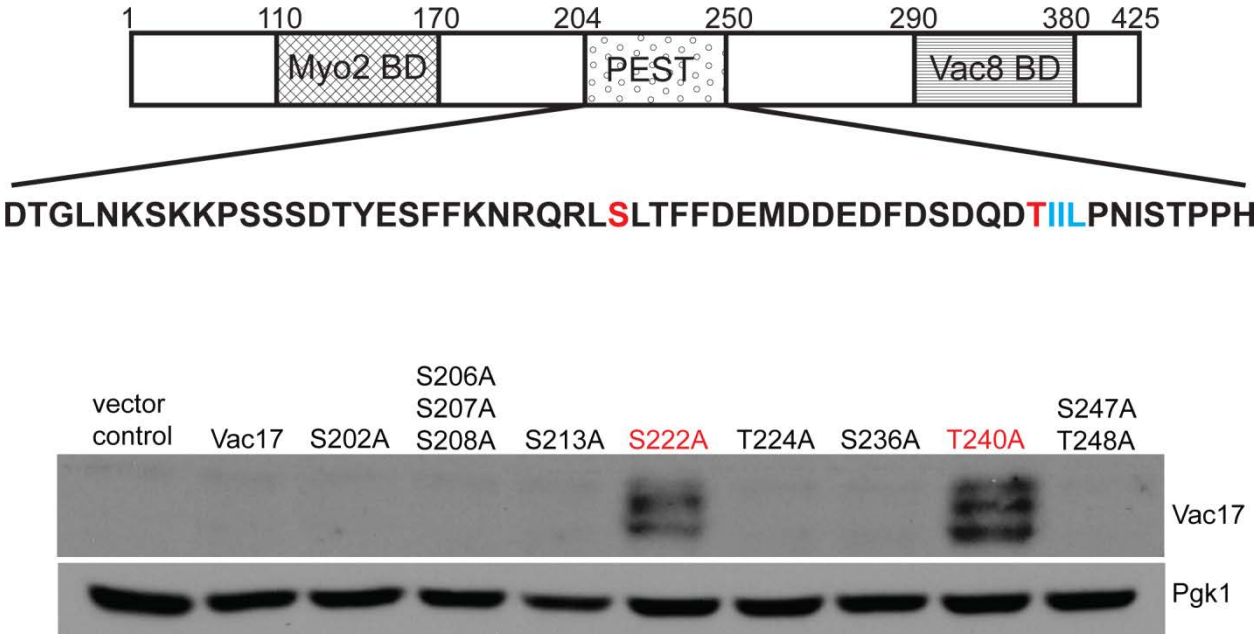

Figure 2.9. Identification of Vac17 residues required for the termination of vacuole movement and Vac17 turnover.

(Top) A schematic representation of Vac17. Vac17 residues 204-250 comprise the PEST sequence (Tang et al., 2003). Red; potential phosphorylation sites required for Vac17 turnover. Blue; FHA binding motif. (Bottom) Western blot analysis of *vac17* point mutants from an alanine scan of all the serine and threonine residues within the Vac17 PEST sequence that cause the accumulation of Vac17. anti-Vac17 antibodies; 1:1,000 dilution. anti-Pgk1 antibodies; 1:10,000 dilution. (Alanine screen and initial western blot analysis were performed by Yutian Peng, western blot shown here was obtained by Richard Yau).

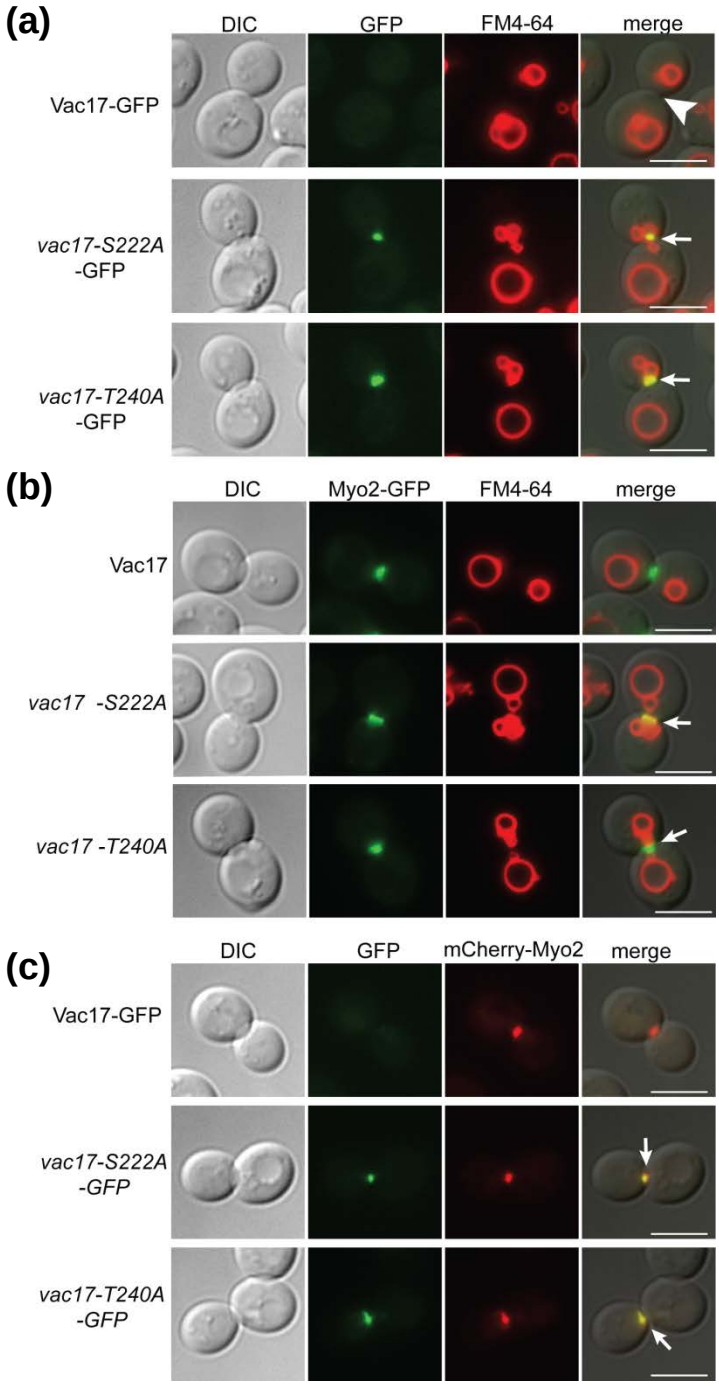

Figure 2.10. *vac17* point mutants fail to dissociate from Myo2.

(a) *vac17-S222A*-GFP and *vac17-T240A*-GFP as well as vacuoles are mis-targeted to the mother bud neck in lage budded cells (arrows). (b) In cells expressing vac17-S222A and vac17-T240A, but not *VAC17*, vacuoles colocalize with Myo2-Venus at the mother-bud neck (arrows). (c) vac17-S222A-GFP and vac17-T240A-GFP, but not Vac17-GFP, colocalize with mCherry-Myo2 at the mother-bud neck (arrows). Bar = 5 μm.

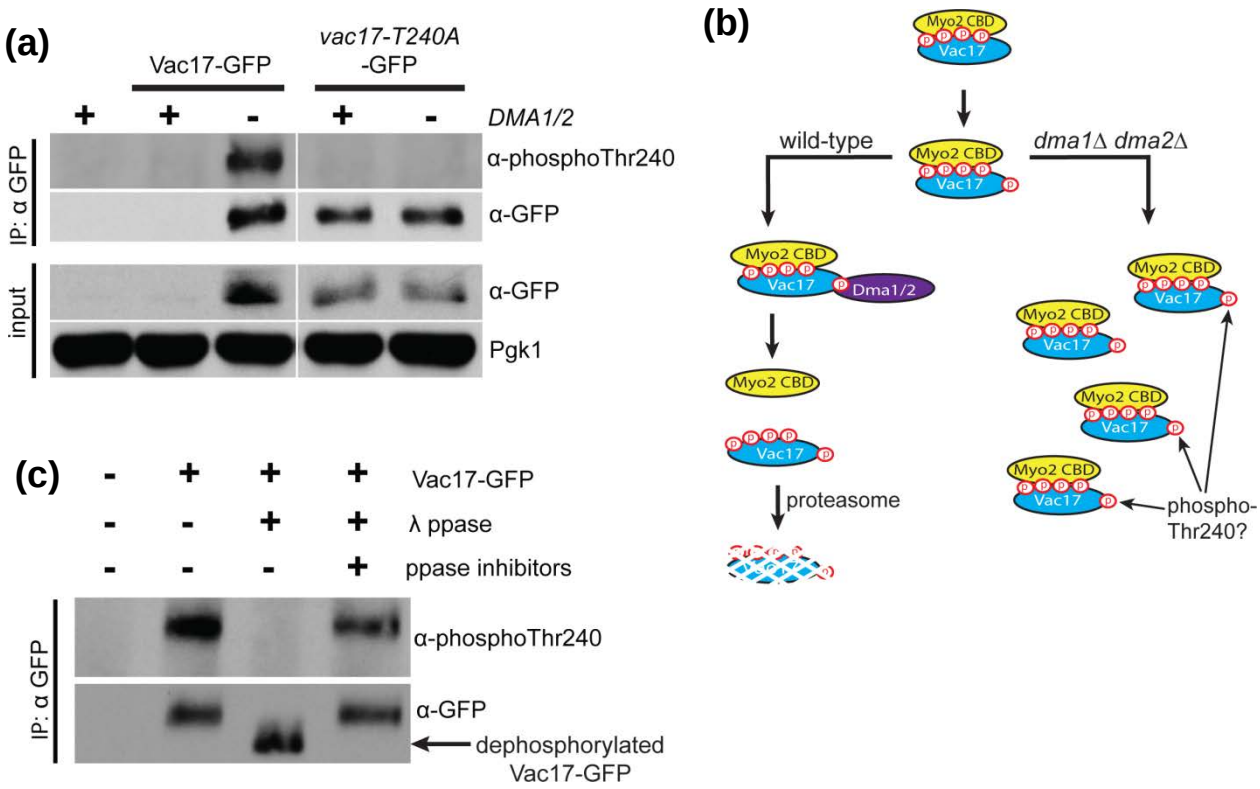

Figure 2.11. Vac17-Thr240 is phosphorylated *in vivo*.

(a) The *dma1Δdma2Δ* mutant has increased Vac17-GFP (input). *vac17-T240A*-GFP levels are higher than Vac17-GFP and are not affected by the deletion of *DMA1* and *DMA2.* Vac17-GFP was immunoprecipitated with anti-GFP antibodies and analyzed using antibodies generated against a peptide with a phosphorylated Thr240 (anti-phThr240). These antibodies recognize Vac17-GFP but not *vac17-T240A*-GFP. (b) Model illustrating the hypothesis that in wild-type cells, Dma1 and Dma2 target phosphorylated Vac17 for degradation. This model predicts that phosphorylated Vac17 would accumulate in a *dma1Δ dma2Δ* mutant. (c) λ-phosphatase (ppase) dephosphorylates Vac17-GFP as indicated by an increase in electrophoretic mobility (arrow). Inhibition of λ-phosphatase activity blocks dephosphorylation. The anti-phosphoThr240 antibody does not recognize dephosphorylated Vac17-GFP. Thus, this antibody is specific for phospho-Thr240 and Vac17-Thr240 is phosphorylated *in vivo*. anti-phospho-Thr240 antibodies; 1:2,500 dilution. anti-GFP antibodies; 1:1,000 dilution.

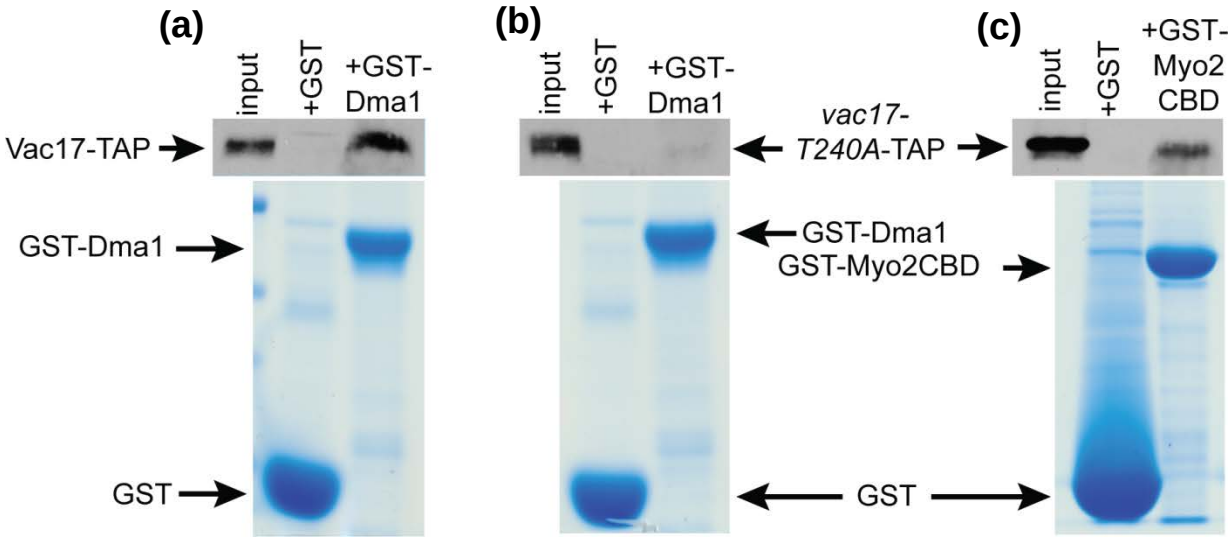

Figure 2.12. Dma1 binds Vac17 *in vitro*.

Recombinant GST-Dma1 was immobilized on GST beads and incubated with yeast cell lysates extracted from strains expressing either *VAC17*-TAP or *vac17-T240A*-TAP from their endogenous loci and with *DMA1/DMA2* deleted. GST-Dma1 binds Vac17-TAP (a) but not *vac17-T240A*-TAP (b). (c) GST-Myo2 cargo binding domain binds *vac17-T240A*-TAP which strongly suggests that *vac17-T240A* folds properly. anti-TAP antibodies; 1:1,000 dilution. Staining; Gelcode Blue stain reagent (Thermo scientific).

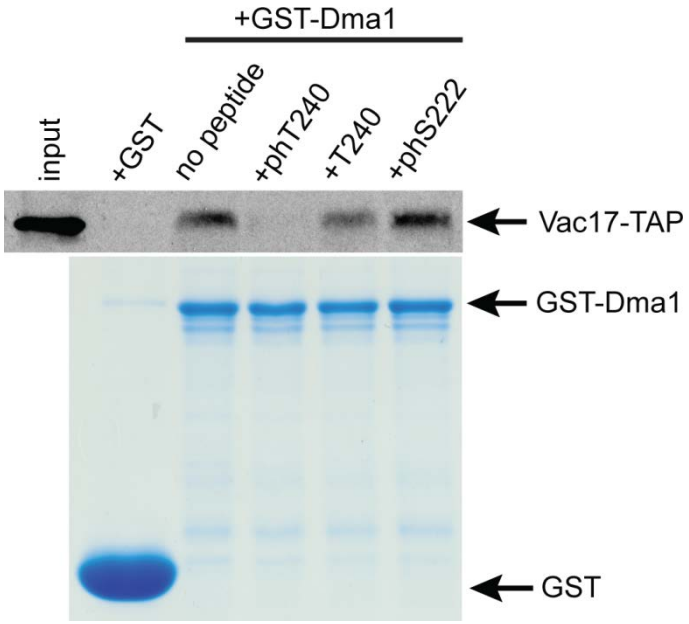

Figure 2.13. Dma1 binds directly to phospho-Thr240 *in vitro*.

Immobilized recombinant GST-Dma1 was pre-incubated with peptides prior to the addition of yeast cell lysates. Addition of a peptide with a central phosphorylated Thr240 blocks GST-Dma1 from binding Vac17-TAP whereas a peptide with an unphosphorylated Thr240 or phosphorylated Ser222 does not block binding. anti-TAP antibodies; 1:1,000 dilution. Staining; Gelcode Blue stain reagent (Thermo scientific).

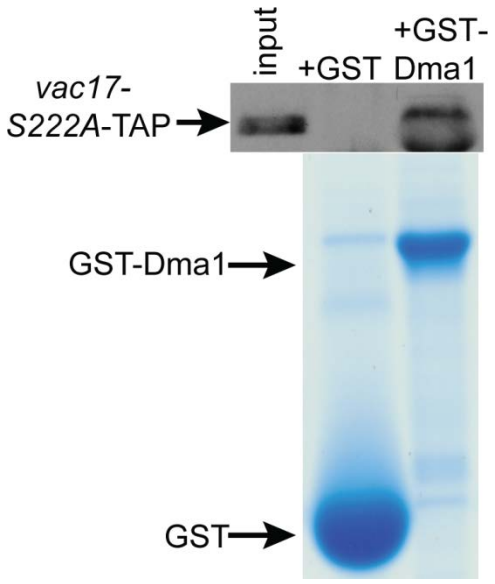

Figure 2.14. Dma1 binds *vac17-S222A in vitro*.

GST-Dma1, but not the GST tag alone, binds *vac17-S222A*-TAP in yeast lysates. anti-TAP antibodies; 1:1,000 dilution. Staining; Gelcode Blue stain reagent (Thermo scientific).

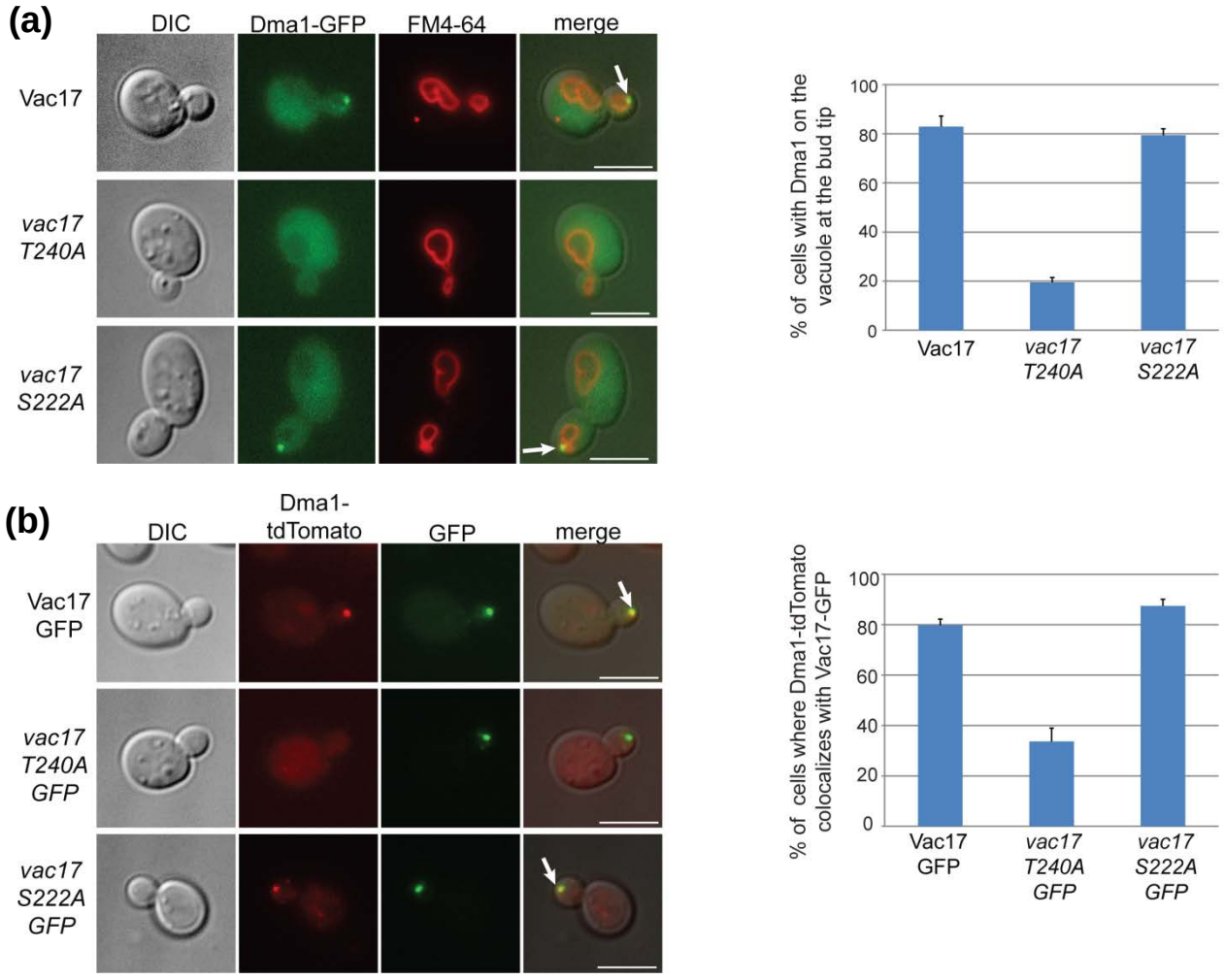

Figure 2.15. Dma1 recruitment to the Myo2/Vac17 vacuole transport complex requires the interaction between Dma1 and Vac17.

(a) (Left) Dma1-GFP localizes to the vacuole at the bud tip (arrows) in cells expressing *VAC17* and *vac17-S222A* but not *vac17-T240A*. (Right) Quantification of the percentage of small budded cells where Dma1-GFP is localized to the bud vacuole. A minimum of 30 cells were counted per experiment for 3 experiments. (b) (Left) Dma1-tdTomato colocalizes with Vac17-GFP and *vac17-S222A*-GFP but not *vac17-T240A*-GFP. Dma1 colocalizes with Vac17 at the bud tip. Arrows; colocalization between Dma1 and Vac17. (Right) Quantification of the percentage of small budded cells where Dma1-tdTomato colocalizes with GFP tagged Vac17 and *vac17* point mutants. A minimum of 13 cells were counted per experiment for 3 experiments. Error bars; SEM. Bar = 5 μm.

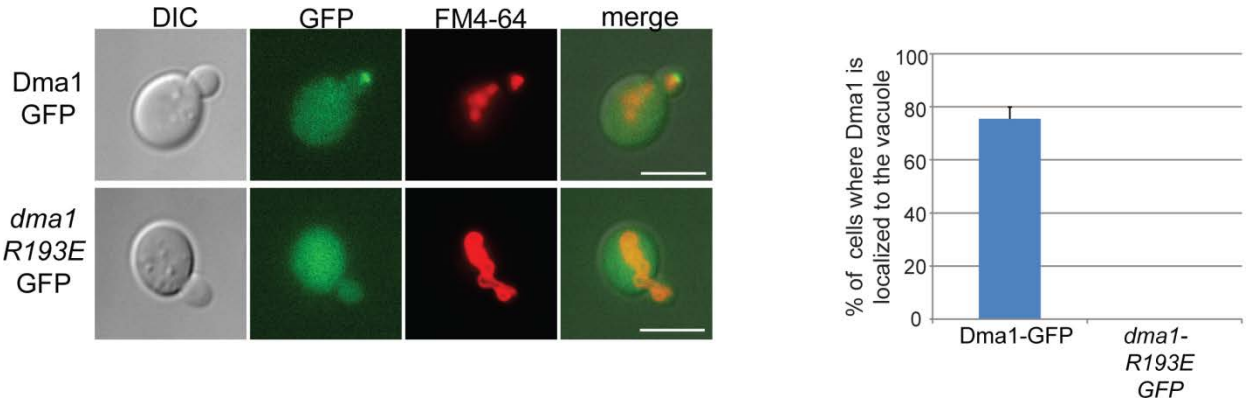

Figure 2.16. The FHA domain of Dma1 is required for the recruitment of Dma1 to the vacuole.

(Left) The *dma1-R193E*-GFP mutant fails to localize to the bud vacuole. (Right) Quantification of the percentage of small budded cells where Dma1-GFP or *dma1-R193E*-GFP localizes to the vacuole. A minimum of 20 cells were counted per experiment for 3 experiments. Z-sections of small budded cells were analyzed. Error bars; SEM. Bar = 5 μm.

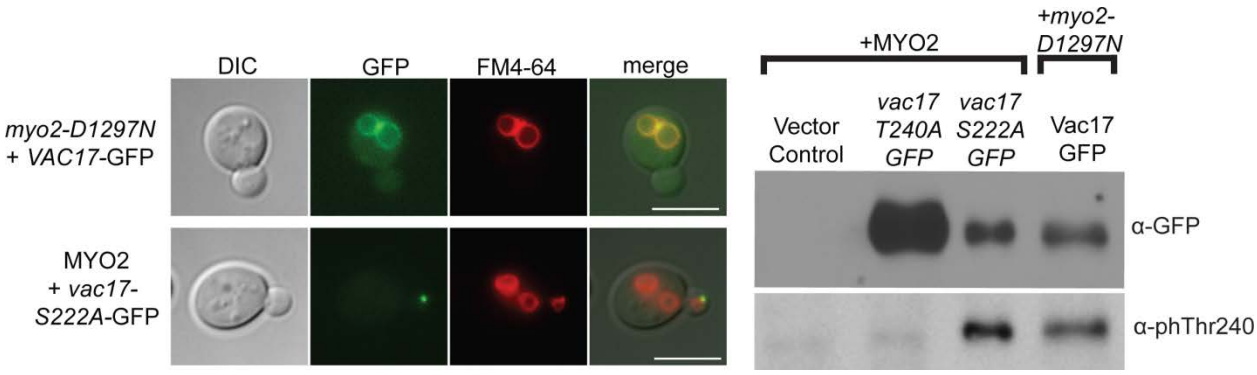

Figure 2.17. Phosphorylation of Vac17-Thr240 does not require Myo2 attachment to the vacuole.

In a *myo2Δvac17Δ* double mutant *myo2-D1297N* and *VAC17*-GFP or *MYO2* and *vac17-S222A*-GFP were co-expressed from plasmids. (Left) In cells expressing *myo2-D1297N*, *VAC17*-GFP is localized throughout the mother vacuole. In cells expressing *MYO2*, *vac17-S222A*-GFP and the vacuole are transported to the bud. (Right) Vac17-GFP in the *myo2-D1297N* mutant and *vac17-S222A*-GFP in cells expressing *MYO2* are phosphorylated at Thr240 to a similar extent. anti-phospho-Thr240 antibodies; 1:2,500 dilution. anti-GFP antibodies; 1:1,000 dilution.

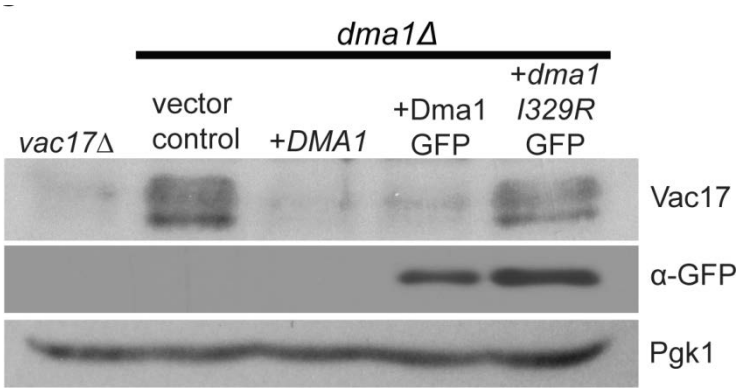

Figure 2.18. Dma1 dependent ubiquitylation is required for Vac17 turnover.

The conserved Ile329 residue, essential for the E3 ubiquitin ligase activity of Dma1, was mutated. The GFP tagged *dma1-I329R* mutant was expressed from a plasmid in the *dma1Δ* mutant and Vac17 levels were tested. Expression of *DMA1* and *DMA1-GFP* but not *dma1-I329R-GFP* or vector control rescues Vac17 levels in the *dma1*Δ mutant. anti-Vac17 antibodies; 1:1,000 dilution. anti-GFP antibodies; 1:1,000 dilution. anti-Pgk1 antibodies; 1:10,000 dilution.

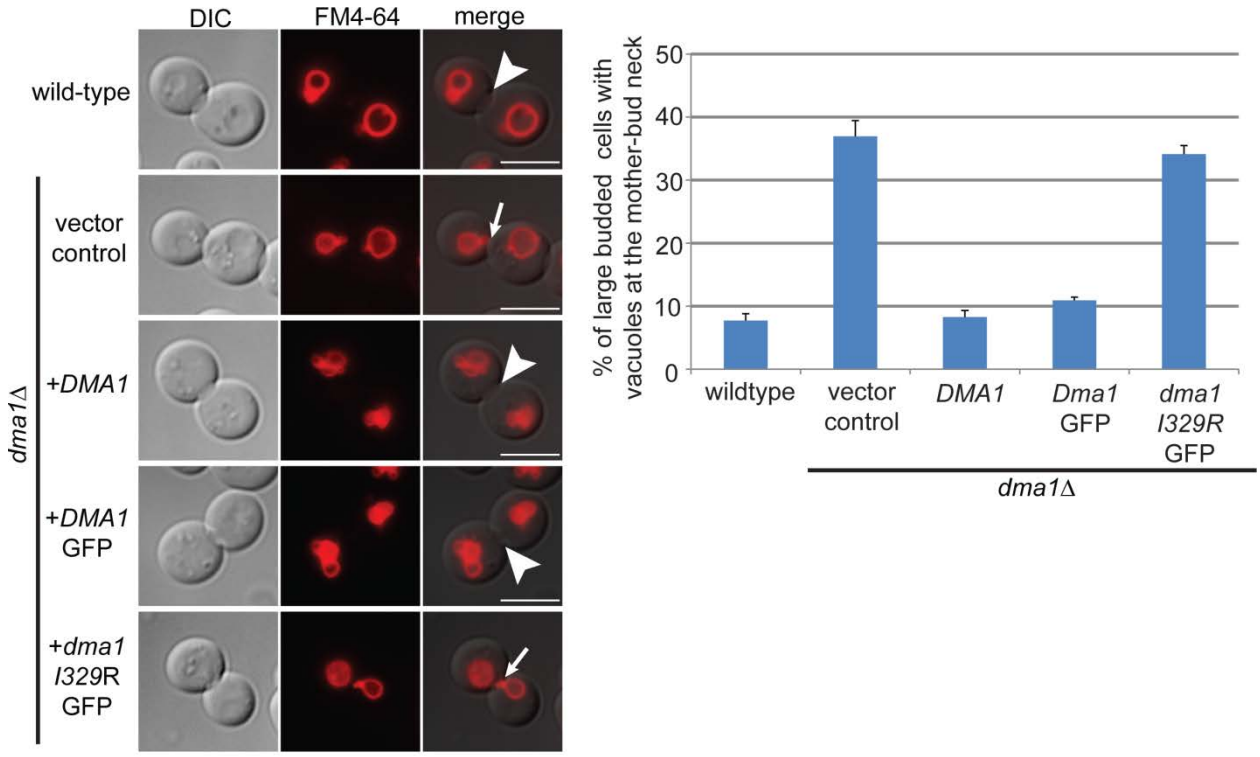

Figure 2.19. The E3 ubiquitin ligase activity of Dma1 is required for the termination of vacuole movement.

(Left) Expression of *DMA1* and *DMA1*-GFP but not a ubiquitylation defective mutant, *dma1-I329R*-GFP, or vector control rescues the termination of vacuole movement in the *dma1Δ* mutant. Arrowheads; vacuoles are deposited properly in the bud and do not accumulate at the mother-bud neck. Arrows; vacuoles are mis-targetd to the mother-bud neck. Bar = 5 μm. (Right) Percentage of large budded cells with vacuoles accumulated at the mother-bud neck in the *dma1Δ* mutant expressing vector control, *DMA1*, *DMA1*-GFP or *dma1-I329R*-GFP. A minimum of 100 cells were counted per experiment for 3 experiments. Error bars; SEM.

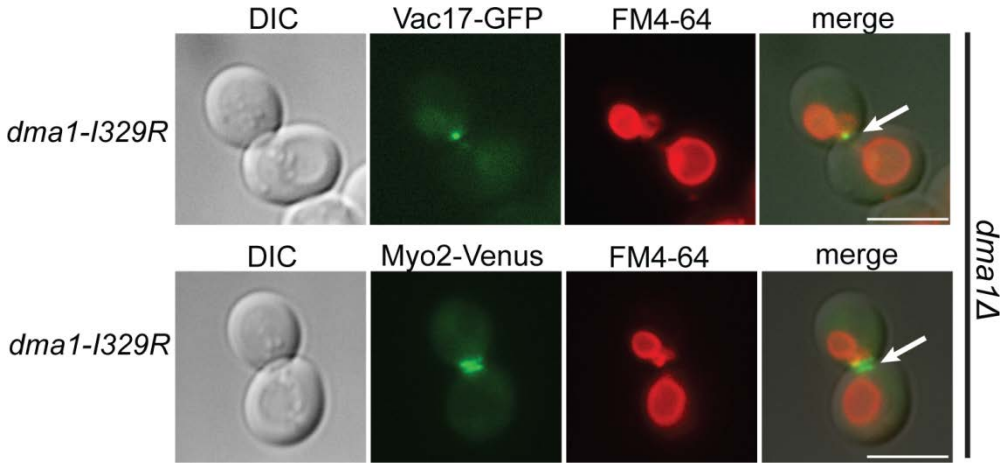

Figure 2.20. The E3 ubiquitin ligase activity of Dma1 is required for the detachment of Vac17 and the vacuole from Myo2.

dma1-I329R was expressed in the *dma1Δ* mutant and the localization of the vacuole with Vac17-GFP or Myo2-Venus was analyzed. In the *dma1-I329R* mutant, in large budded cells, (top) Vac17-GFP and the vacuole are mis-targeted to the mother-bud and (bottom) the vacuole colocalizes with Myo2-Venus at the mother-bud neck (arrows). Bar = 5 μm.

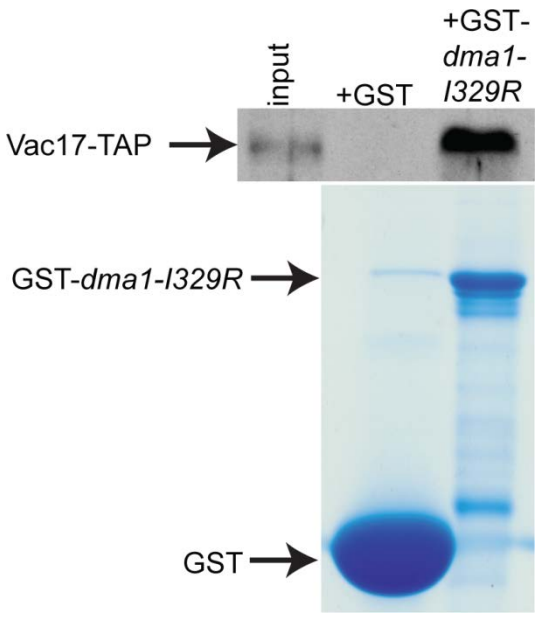

Figure 2.21. The enzymatically inactive *dma1* mutant binds Vac17 *in vitro*.

Immobilized recombinant GST-*dma1-I329R* binds Vac17-TAP in yeast cell lysates. anti-TAP antibodies; 1:1,000 dilution. Staining; Gelcode Blue stain reagent (Thermo scientific).

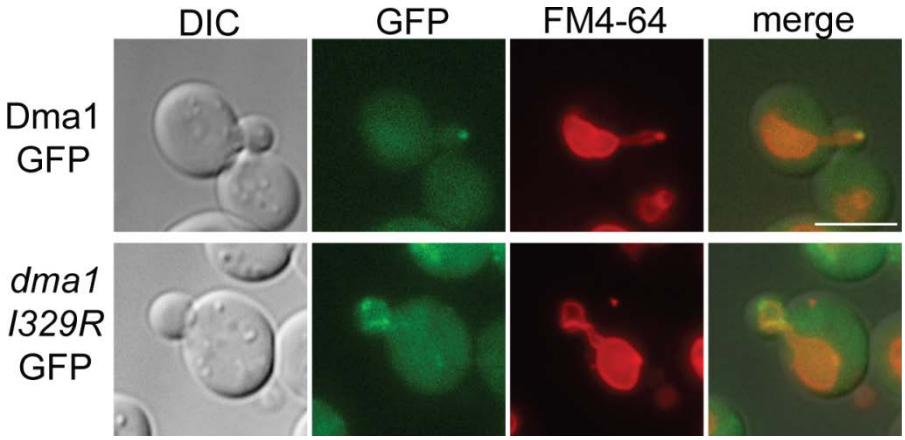

Figure 2.22. *dma1-I329R*-GFP localizes to a broader region of the vacuole.

DMA1-GFP or *dma1-I329R*-GFP was expressed in the dma1 mutant and their localization was analyzed. *dma1-I329R*-GFP localizes to a broader area on the bud vacuole. Bar = 5 μm.

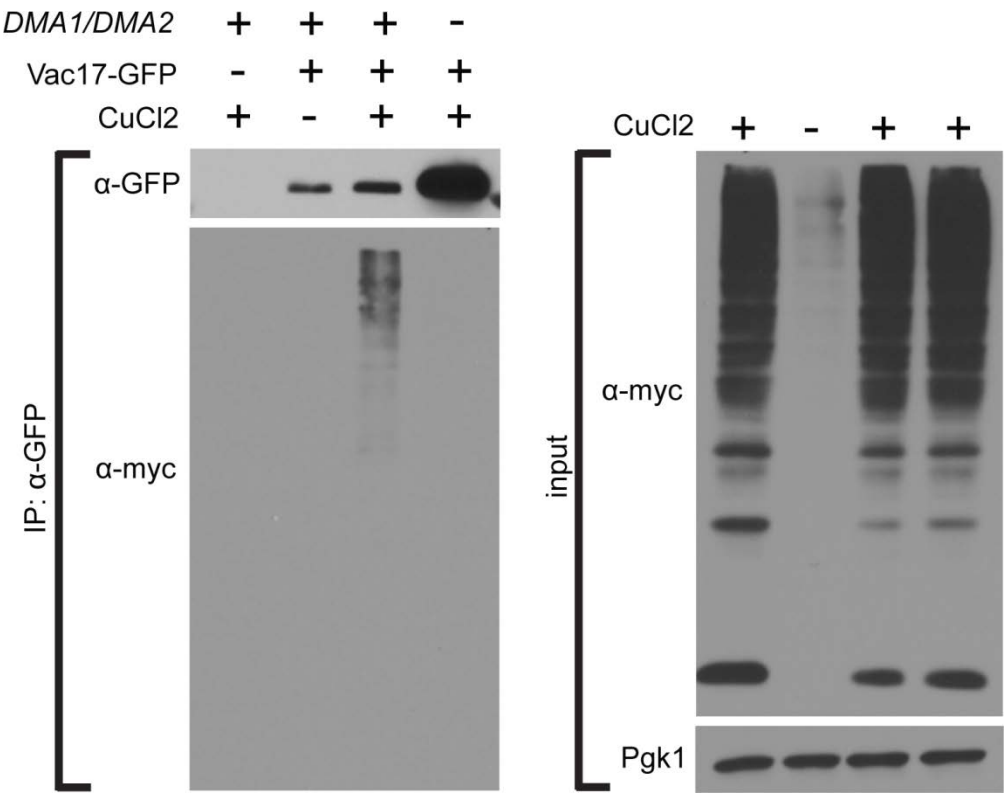

Figure 2.23. Dma1 and Dma2 are required for Vac17 ubiquitylation *in vivo*.

A plasmid encoding *VAC17*-GFP under an ADH promoter and a plasmid encoding myc-Ub under a CUP1 promoter were co-transformed into wild-type or *dma1Δdma2Δ* cells. myc-Ub over-expression was induced with the addition of 100μM $CuCl_2$. Vac17-GFP was immunoprecipitated with anti-GFP antibodies and analyzed with anti-myc antibodies. Anti-myc antibodies recognize myc-Ub conjugated to Vac17-GFP from cells over-expressing myc-Ub. Deletion of *DMA1/DMA2* results in the accumulation of Vac17-GFP that is not recognized by the anti-myc antibodies. anti-GFP antibodies; 1:1000 dilution. anti-myc antibodies; 1:2,000 dilution. anti-Pgk1 antibodies; 1:10,000 dilution.

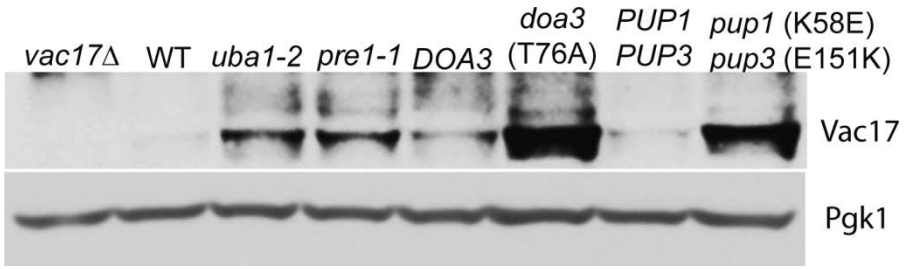

Figure 2.24. The Ub-proteasome system is required for Vac17 degradation.

In the *uba1-2* E1 mutant and in the *pre1-1*, *doa3-T76A* and *pup1-K58E/pup3-E151K* proteasome mutants, Vac17 levels are elevated compared to the wild-type. anti-Vac17 antibodies; 1:1000 dilution. anti-Pgk1 antibodies; 1:10,000 dilution.

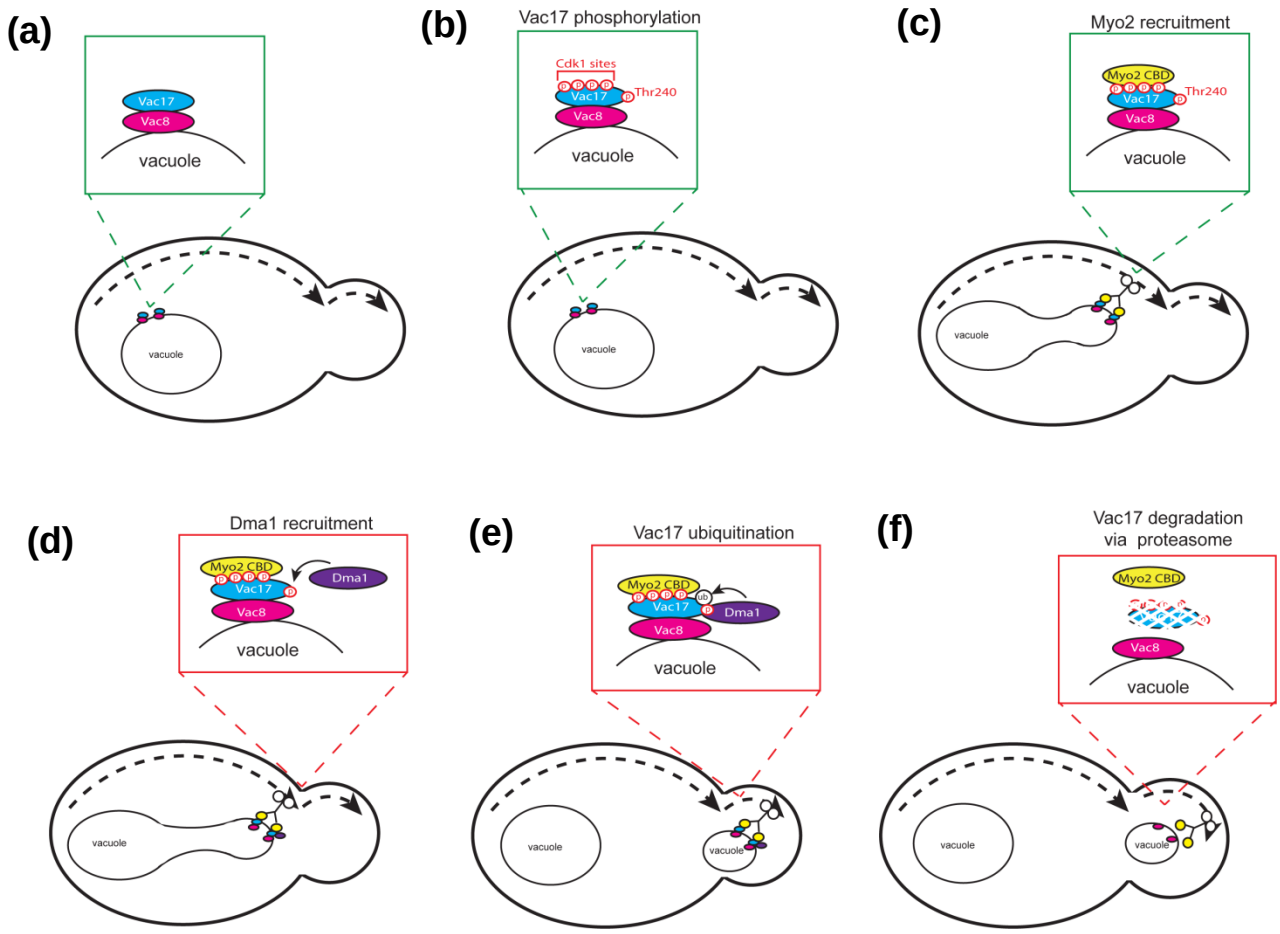

Figure 2.25. Model for the regulation of vacuole transport.

(a-b) Vac17 is phosphorylated at Thr240 as well as at four Cdk1 sites. (c) Myo2 binds Vac17 and attaches to the vacuole in the mother cell to initiate transport. (d) After assembly of the Myo2/Vac17/Vac8 transport complex, Dma1 is recruited to the vacuole via binding directly to Vac17 at phospho-Thr240. (e-f) Vac17 ubiquitylation by Dma1 targets Vac17 for degradation via the proteasome which detaches the vacuole from Myo2 and terminates vacuole transport. The timing of these late events remains to be determined. However, note that the vacuole remains associated with Dma1 and Myo2 until after the resolution of the segregation structure, the connection between the mother and bud vacuoles.

CHAPTER III

Discussion

Within a single cell type, myosin V transports multiple organelles. Accurate transport requires that myosin V attaches to cargoes at their original locations and detaches from cargoes at their destinations. The accurate release of organelles from myosin V is critical for their proper subcellular location (Tang et al., 2003). Our findings suggest that the detachment of cargoes from myosin V occurs in multiple steps along the entire route of cargo transport. Phosphorylation of Vac17-Thr240 occurs in the mother cell and sets up the termination of vacuole transport which occurs later in the bud. Vac17-Thr240 is phosphorylated at the same cellular location where Cdk1 phosphorylates Vac17 at S119, T149, S178, and T248 to recruit Myo2, which initiates vacuole transport (Peng and Weisman, 2008). Because phosphorylation of Vac17-Thr240 does not require Myo2, it is likely that phosphorylation of the 4 Cdk1 sites as well as Thr240 occur concurrently prior to the initiation of vacuole transport. Moreover, phosphorylation of Thr240 likely does not require Cdk1 phosphorylation of Vac17. In the *vac17-S119/T149/S178/T248A* mutant, vacuoles that are transported to the bud undergo normal release from Myo2 (data not shown).

Our results demonstrate that Thr240 phosphorylation creates a binding site on Vac17 that is critical for the recruitment of Dma1 to the vacuole. Intriguingly, while phosphorylation of Vac17-Thr240 occurs in the mother cell and does not require the attachment of Myo2 to the vacuole, Dma1 is first observed on the vacuole in the bud

and its recruitment to the vacuole requires Myo2. This suggests that either Dma1 recognizes the intact Myo2/Vac17/Vac8 vacuole transport or that Dma1 is recruited to the vacuole in the bud. Furthermore, these results suggest that Thr240 phosphorylation is required but not sufficient for Dma1 recruitment. Moreover, our results suggest that the regulated recruitment of Dma1 to the vacuole is critical for Vac17 degradation.

Notably, after Dma1 is recruited to the vacuole, there is a delay in the mechanism which terminates vacuole transport. Dma1 moves with the vacuole to the bud tip and persists on the vacuole after the bud vacuole separates from the mother vacuole. This suggests that Dma1 activity is regulated so that termination of vacuole transport is coordinated with the resolution of the vacuole segregation structure. Overall, our findings suggest that Dma1 recruitment and function are modulated by at least three events: 1) Vac17 phosphorylation on Thr240, 2) Myo2 attachment to the vacuole and 3) the resolution of the segregation structure.

We further find that Dma1 and Dma2 function in the ubiquitylation of Vac17 *in vivo*. Dma1 dependent ubiquitylation targets Vac17 for degradation via the proteasome which releases the vacuole from Myo2 (Figure 2.25). In addition to the vacuole, we found that the termination of peroxisome transport also requires *DMA1* and *DMA2* (Figure 2.5). Like the vacuole, peroxisomes are transported by Myo2 and are attached to Myo2 via a cargo adaptor, Inp2. The mechanisms that detach the vacuole from Myo2 also likely terminate the transport of peroxisomes. Together, these studies suggest that the degradation of cargo adaptors by the Ub-proteasome system may be a common mechanism to release cargoes from molecular motors.

Myo2 transports multiple cargoes

In addition to the vacuole, Myo2 cargoes include peroxisomes, the mitochondria, secretory vesicles, microtubules (MTs) and the late Golgi. The mechanisms which detach the vacuole from Myo2 may be similar to those which regulate the transport of other Myo2 cargoes. Consistent with this hypothesis, recent studies demonstrate that Vac17 and other cargo adaptors are regulated via similar mechanisms.

Vac17 levels and phosphorylation oscillate with the cell cycle. This oscillation contributes to the coordination of vacuole transport with the cell cycle (Peng and Weisman, 2008; Tang et al., 2003). Intriguingly, the levels of the peroxisome adaptor, Inp2, and microtubule adaptor, Kar9, also oscillate with the cell cycle. Moreover, Kar9, Inp2 and Ypt11 are phosphorylated. Like Vac17, Kar9 is a substrate of Cdk1, Cdk1 dependent phosphorylation ensures asymmetrical loading of Kar9 onto MTs which are transported to the bud by Myo2 (Fagarasanu et al., 2006; Fagarasanu et al., 2009; Lewandowska et al., 2013; Liakopoulos et al., 2003).

Bud-specific degradation of Vac17 is required for the accurate placement of the vacuole in the bud. Vac17 levels are elevated in *myo2* point mutants that are defective in vacuole transport. This suggests that Vac17 is degraded in the bud. Notably, Inp2 and Mmr1 levels are elevated in *myo2* mutants which are defective in peroxisome and mitochondria transport, respectively (Eves et al., 2012; Fagarasanu et al., 2009). Therefore, Inp2 and Mmr1 are also degraded via bud-specific mechanisms. Moreover, the termination of vacuole and peroxisome transport requires *DMA1/DMA2*. These observations suggest that Vac17 and other Myo2 cargo adaptors are regulated via similar mechanisms.

Myosin V transport in yeast and vertebrates

Myosin V motors are present in virtually all eukaryotic organisms. *S. cerevisiae* express Myo2 and Myo4. In *Schizosaccaromyces pombe*, there are also 2 myosin V motors, Myo51 and Myo52. Unlike Myo2 and Myo4, there is no evidence to suggest that either Myo51 or Myo52 transport organelle cargoes. Myo51 is a component of the contractile actomyosin ring and functions in cytokinesis. Myo52 functions in cytokinesis as well as cell wall deposition and cell growth (Win et al., 2001). Myo52 also regulates vacuole morphology and distribution in an MT dependent manner (Mulvihill et al., 2001). It is unclear whether the mechanisms which regulate Myo2 and Myo4 transport are similar to those which regulate Myo51 and/or Myo52.

The differences in myosin V function in *S. cerevisiae* versus *S. pombe* are further highlighted by the fact that cargo adaptors which attach Myo2 and Myo4 to cargoes in *S. cerevisiae* are not conserved in *S. pombe*. For example, Vac17, Inp2, Mmr1 and She2 are present only in *S. cerevisiae* and closely related yeast species. These cargo adaptors function solely in the attachment of myosin V to cargoes. Cargo adaptors bind both myosin V and a second protein found on the cargo. For example, Vac17 binds both Myo2 and Vac8, a vacuolar protein. While the only known role of Vac17 is in vacuole transport, Vac8 functions in other vacuole related processes. Notably, Vac8 and other proteins involved in cargo transport that have additional roles in other pathways tend to be conserved (Mast et al., 2012). This rapid evolution of cargo adaptors enables organisms to evolve different mechanisms of organelle transport while leaving organelle related pathways intact.

Although Vac17 is not conserved, the mechanisms which regulate Vac17 and

vacuole transport may be similar to those which regulate other myosin V cargoes in higher eukaryotes. Mammals have 3 class V myosins, myosin Va, Vb and Vc (Desnos et al., 2007; Hammer and Sellers, 2011; Weisman, 2006). Myosin V motors are present in diverse cell types and transports different cargoes. For example, myosin V transports melanosomes in melanocytes, the ER in Purkinje neurons and recycling endosomes in epithelial cells (Hammer and Sellers, 2012). Like yeast Myo2, mammalian myosin V attaches to cargoes via cargo specific adaptor proteins.

The mammalian lysosome is analogous to the yeast vacuole. However, it is unknown whether lysosomes undergo myosin V dependent transport. Thus, it is difficult to predict whether the mechanisms which regulate vacuole transport are similar for the lysosome. In contrast, melanosomes, pigment containing organelles that are similar to lysosomes, are well characterized myosin V cargoes. Myosin Va transports melanosomes via binding the adaptor, melanophilin, and Rab27a (Fukuda et al., 2002; Strom et al., 2002; Wu et al., 2002). Notably, melanophilin contains 3 PEST sequences which are important for melanophilin turnover and melanosome transport (Fukuda and Itoh, 2004). Intriguingly, western blot analyses show that melanophilin, like Vac17, runs at a higher molecular weight than predicted, suggesting that melanophilin may be phosphorylated (Wu et al., 2002). Given the similarities between Vac17 and melanophilin, we propose that the mechanisms that regulate Vac17 and the termination of vacuole transport may be similar to those that regulate the detachment of other organelles from myosin V in higher eukaryotes.

Like *S. cerevisiae*, the mammalian genome encodes 2 proteins that contain both FHA and RING domains, Rnf8 and Chfr. Chfr also contains a poly-ADPribose binding

zinc (PBZ) finger. While Rnf8 and Chfr are checkpoint proteins, their known functions differ from Dma1 and Dma2. Rnf8 is part of the DNA Double-Strand Break (DSB) repair pathway. Upon DNA damage, Rnf8 accumulates at the breakage site and ubiquitylates exposed histones, H2A and H2AX, which then recruits downstream effectors of the DSB repair pathway to the site of DNA breakage (Huen et al., 2007; Mailand et al., 2007). Chfr inhibits mitotic entry in response to a range of microtubule stress agents such as nocodazole and taxol (Chaturvedi et al., 2002; Scolnick and Halazonetis, 2000). Recent studies suggest that Chfr, with Rnf8, functions in the DSB repair pathway as well (Wu et al.). While the FHA and RING domains of Rnf8 and Chfr exhibit the greatest sequence homology, they share little homology with the FHA and RING domains of yeast Dma1 and Dma2 (Brooks et al., 2008). It remains unclear as to whether Rnf8 or Chfr are the mammalian homologues of Dma1 and Dma2 and whether Rnf8 or Chfr functions in the termination of myosin V dependent transport.

Regulation of the termination of myosin V transport

In *S. cerevisiae*, Myo2 actively transports cargoes throughout the cell cycle. The itineraries for Myo2 cargoes overlap but are not identical. For example, Myo2 transports the vacuole and secretory vesicles from the mother cell to the bud early in the cell cycle. However, after vacuole transport terminates, Myo2 continues to transport secretory vesicles to the mother-bud neck. Our studies show that the modulation and degradation of Vac17 directly regulate vacuole transport. Because Myo2 and Vac8 have functions other than vacuole transport, specifically targeting Vac17 for degradation terminates vacuole transport without perturbing other processes involving Myo2 or Vac8.

Evidence from *Xenopus laevis* suggests that, in addition to cargo adaptors, the cargo binding domain of myosin V may also play a critical role in the detachment of cargoes. In Xenopus, Calcium/calmodulin-dependent protein kinase II (CaMKII) directly phosphorylates the myosin V cargo binding domain (Karcher et al., 2001). This phosphorylation event causes the release of the melanosome from myosin V. Thus, the modulation of both myosin V and its cargo adaptor followed by degradation of the cargo adaptor may be common mechanisms that regulate the termination of myosin V transport.

In *S. cerevisiae* Myo2 actively transports organelles to different locations and at distinct times during the cell cycle. Therefore, it is important for Myo2 to attach to a subset of organelles while releasing others. In this situation, it is advantageous to regulate the cargo adaptors which link Myo2 to specific cargoes. In contrast, myosin V transport ceases during cell division in *Xenopus laevis* melanophores. Since myosin V transport is globally inhibited, it may be advantageous to directly regulate the motor instead of targeting individual cargo adaptors.

Dma1 and Dma2 regulate multiple cell cycle coordinated processes

The segregation of chromosomes is critical to cell division. In yeast, spindle pole bodies (SPBs) organize the microtubules which attach to the kinetochores. Correct attachment of kinetochores to the mitotic spindle and proper alignment of the sister chromatids along the metaphase plate ensures that both mother and daughter cells receive the proper complement of chromosomes (Jaspersen and Winey, 2004). The spindle assembly checkpoint inhibits the metaphase-anaphase transition until the correct kinetochore-spindle attachments are achieved. Successful segregation of chromosomes

activates a signaling pathway that triggers mitotic exit and cytokinesis. This pathway originates from the SPB and is referred to as the mitotic exit network (MEN) in *S. cerevisiae* and the septation initiation network (SIN) in *S. pombe* (Seshan and Amon, 2004).

In *S. pombe*, Dma1 participates in the spindle assembly checkpoint. If spindle assembly is compromised, Dma1 inhibits mitotic exit. In this situation, Dma1 ubiquitylates the SPB associated scaffold protein, Sid4. Dma1 dependent ubiquitylation of Sid4 prevents the recruitment of the polo-like kinase, Plo1, to the SPBs (Guertin et al., 2002; Johnson and Gould, 2011; Murone and Simanis, 1996). Plo1 is an activator of the septation initiation network and inhibition of Plo1 recruitment to the SPBs prevents mitotic exit and cytokinesis.

In *S. cerevisiae*, Dma1 and Dma2 inhibit mitotic exit in response to mis-positioned spindles (Fraschini et al., 2004). Unlike in *S. pombe*, Dma1 and Dma2 do not directly inhibit the mitotic exit network, but rather are upstream regulators of the spindle position checkpoint. Dma1 and Dma2 recruit the kinase Elm1 to the mother-bud neck where it regulates Kin4, a kinase that activates Bfa1, a direct inhibitor of the mitotic exit network. Moreover, Dma1 and Dma2 are important for proper septin ring assembly which in turn is required for proper spindle positioning and for cytokinesis (Chahwan et al., 2013; Fraschini et al., 2004). Further studies demonstrate that Dma1 and Dma2 regulate the levels of Swe1, a kinase which regulates the G_2/M transition, and Pcl1, a cyclin for Pho85 required for progression through G_1 (Chahwan et al., 2013; Raspelli et al., 2011). Thus, Dma1 and Dma2 function in regulating cell cycle progression.

Given that Dma1 and Dma2 regulate multiple cell cycle processes, it is tempting to speculate that these E3 ubiquitin ligases may coordinate the termination of myosin V transport with other cell cycle events such as mitotic exit and/or cytokinesis. Ensuring that the termination of Myo2 cargo delivery occurs prior to mitotic exit and cytokinesis is likely important to ensure that the daughter cell receives all the components required for viability.

CHAPTER IV

Future directions

These studies demonstrate that post-translational modifications of Vac17 directly regulate Vac17 degradation and the termination of vacuole transport. We found that phosphorylation of Vac17-Thr240 recruits the E3 ubiquitin ligase Dma1 to the vacuole transport complex. Dma1 ubiquitylation of Vac17 is required for detachment of the vacuole from Myo2 and for Vac17 turnover, which likely occurs via the proteasome. These studies provide insights into the mechanisms which terminate vacuole transport. However, several questions remain.

Is Dma1 recruited to the vacuole specifically in the bud?

In the *myo2-D1297N* mutant, Dma1-GFP is not recruited to the mother vacuole. Moreover, Dma1-3xGFP is first observed on the vacuole in the bud. One possibility is that Dma1 is recruited specifically to the bud vacuole. Alternatively, Dma1 may recognize the intact vacuole transport complex and initially bind Myo2/Vac17/Vac8 in the mother cell. Based on *in vivo* organelle tracking studies, the rate of myosin V transport averages ~3μm/s, thus after Myo2 attaches to the vacuole, the vacuole moves into the bud within seconds, making it difficult to ascertain whether Dma1 initially localizes to the vacuole in the mother. To address this question, recruitment of Dma1 to the vacuole can be tested under conditions where the vacuole transport complex is

assembled, but the vacuole is not transported to the bud. Over-expression of *Myo2-tail∆AflII*, a mutated Myo2 CBD which binds the vacuole but not secretory vesicles, causes a defect in vacuole transport by competing with endogenous Myo2 for Vac17 binding (Catlett et al., 2000). This predicts that a *Myo2-tail∆AflII*/Vac17/Vac8 complex is assembled on the mother vacuole but because *Myo2-tail∆AflII* lacks a motor domain, the vacuole does not move into the bud. We can test whether over-expression of *Myo2-tail∆AflII* results in the localization of Dma1 to the mother vacuole. Because *Myo2-tail∆AflII* does not bind secretory vesicles, over-expression of this construct is not lethal.

Is Dma1 activated at the bud tip?

After Dma1 localizes to the vacuole, there is a delay in the termination of vacuole transport and the vacuole continues to move to the bud tip (Figure 2.7). This suggests that Dma1 activity is regulated. Another factor which localizes to the vacuole in the bud is Cla4, a p21activated kinase. Furthermore, Cla4 functions in Vac17 degradation and the termination of vacuole transport (Bartholomew and Hardy, 2009). These observations raise the intriguingly hypothesis that Cla4 functions in the termination of vacuole transport via activating Dma1 at the bud tip. To address this question, the colocalization of Cla4-GFP with Dma1-tdTomato will be tested. Whether Dma1 is phosphorylated in a Cla4 dependent manner will also be tested.

Is Vac17 localization perturbed in the *dma1-I329R* mutant?

The GFP tagged *dma1-I329R* localizes to a broader region of the bud vacuole (Figure 2.22). The recruitment of Dma1 to the vacuole is dependent on the interaction between

Dma1 and Vac17. Moreover, Dma1 colocalizes with Vac17 on the vacuole (Figure 2.15). Therefore, the localization of *dma1-I329R*-GFP may be a result of Vac17 localizing to a broader region on the vacuole in this mutant. To explore this question, Vac17-GFP localization will be tested in cell expressing *dma1-I329R*.

Is vacuole inheritance required for spindle positioning or spindle positioning checkpoint activation?

Given that Dma1 and Dma2 function in spindle positioning, the spindle positioning checkpoint and the termination of vacuole transport, we hypothesize that these cell cycle processes may be coordinated. However, we found that in the *vac17Δ* mutant, spindle positioning is not perturbed (data not shown). This suggests that vacuole inheritance and spindle positioning are separate processes. However, it is possible that vacuole transport is required for Dma1/Dma2 to function in the spindle positioning checkpoint. To address this question, activation of a checkpoint arrest will be tested in a *kar9Δvac17Δ* mutant. In the absence of Kar9, which functions in spindle positioning, a subset of cells will have misaligned spindles and will arrest in mitosis in a Dma1/Dma2 dependent manner. If Vac17 is required for the checkpoint function of Dma1/Dma2, the absence of Vac17 will enable cells with mis-aligned spindles to exit mitosis and continue into cytokinesis.

Does a defect in the termination of vacuole transport trigger a checkpoint arrest?

The termination of vacuole transport is regulated by checkpoint proteins Dma1 and Dma2. This raises the hypothesis that a defect in the termination of vacuole transport

may activate a Dma1/Dma2 mediated checkpoint arrest. To address this question, cells expressing *vac17-T240A* will be tested for a delay in mitotic exit and cytokinesis. If these cells progress normally through the cell cycle, this would suggest that a defect in the termination of vacuole transport does not activate checkpoint arrest.

What other factors are required for the termination of vacuole transport?

To identify additional factors required for the detachment of the vacuole from Myo2, we can perform a systematic and high content microscopy based screen to identify all non-essential genes required for Vac17 abundance and localization. Vac17-GFP will be introduced into a library of mutants where each non-essential gene is individually deleted. High throughput fluorescence microscopy will determine the abundance and localization of Vac17-GFP. Mutants with elevated GFP fluorescence will be further analyzed. Vac17 levels will be tested in these mutants via western blot. The corresponding genes can be tagged with GFP and the localizations of the GFP tagged fusion protein can be determined. Furthermore, the vacuoles in these mutants will be labeled with FM4-64 and vacuole transport will also be analyzed. Hypomorphic alleles of all essential genes, with reduced levels of expression, can also be tested. This unbiased screen will likely identify novel factors which regulate the detachment of the vacuole from Myo2.

CHAPTER V

Methods

Yeast Strains, Plasmids and Media

Yeast cultures were grown in yeast extract peptone dextrose (YEPD) containing 1% yeast extract, 2% peptone and 2% dextrose or synthetic complete (SC) media lacking the indicated amino acid(s) at 24^{O}C unless specified. Yeast strains and plasmids listed in Tables S1 and S2 respectively.

Western Blot Analysis and Immunoprecipitation Experiments

Cells were lysed in chilled 1 ml 0.2 M NaOH/ 0.2% β-mercaptoethanol and incubated on ice for 10 min. 100 µl trichloroacetic acid (TCA) was added to the lysates and incubated on ice for 5 min. Precipitated proteins were harvested via centrifugation at 12,000 rpm for 5 min. Pellets were resuspended in 100 µl 2X SDS sample buffer, 20 µl of 1 M Tris base (pH 11) was then added and the samples were heated at 75^{O}C for 10 min (Peng and Weisman, 2008). Protein samples were analyzed via immunoblot.

For immunoprecipitations, TCA precipitated proteins were pelleted and washed with acetone. The dried protein pellets were resuspended in 200 µl urea cracking buffer (6 M urea, 1% SDS, 50 mM Tris-HCl, pH 7.5) and heated at 75^{O}C for 10 min. 1.8ml TWIP buffer (50 mM Tris-HCl, pH 7.5, 150 mM NaCl, 0.5% Tween 20, 0.1 mM EDTA) containing 1 mM Na_3VO_4 and 1X protease inhibitor cocktail (Sigma) was added to the resuspended protein. Undissolved proteins were pelleted via centrifugation. 4 µg of

mouse anti-GFP antibodies (Roche) was added to the supernatant and incubated with agitation at 4^{O}C, overnight. 50 µl of protein G beads (Sigma) washed with TWIP buffer was added and incubated with agitation at 4^{O}C for 1 hour. Beads were collected via centrifugation and washed with TWIP buffer. Bound proteins were analyzed via immunoblot.

For dephosphorylation of Vac17-GFP, Protein G beads were collected via centrifugation and washed 3 times with TWIP buffer without EDTA. The beads were resuspended in 1X λ-ppase buffer containing 1X protease inhibitor cocktail (Sigma) and 10 mM $MnCl_2$. Either water, λ-ppase (400 units, New England Biolabs) or λ-ppase plus phosphatase inhibitors (100 mM NaF, 10 mM Na_3VO_4, 50 mM EDTA, 20 mM β-glycerophosphate and 20 mM sodium pyrophosphate) were added to the samples. Phosphatase reactions were performed in 100 µl and incubated at 30^{O}C for 1 hour. Reactions were terminated by addition of 50 µl 2X SDS sample buffer and heated at 75^{O}C for 10 min.

For immunoblot analyses, mouse anti-GFP (1:1,000; Roche), rabbit anti-GFP (1:1,000; abcam), rabbit anti-TAP (1:1,000; Thermo Scientific), mouse anti-Pgk1 (1:10,000; Invitrogen), sheep anti-Vac17 (1:1,000) and rabbit anti-phosphoThr240 (1:2,500) antibodies were used.

In Vitro Binding and Competition Experiments

Expression of GST tagged fusion proteins from BL21 star DE3 cells was induced with 0.4 mM IPTG (Denville Scientific); 16^{O}C overnight. Cells were resuspended in 50 mM Tris-HCl, pH 7.5, 1 mM EDTA, 4 mM $MgCl_2$, 10% glycerol, 1 M NaCl, 5 mM DTT, 1 mM Pefabloc and Complete EDTA-free protease inhibitor cocktail (Roche) and lysed via sonication. An equal amount of lysis buffer without NaCl was added to the clarified

lysates and incubated with glutathione Sepharose beads (GE Healthcare). Immobilized GST fusion proteins were washed with wash buffer (50 mM Tris-HCl, pH 7.5, 4 mM $MgCl_2$, 10% glycerol, 0.5 M NaCl and 1 mM DTT and then with 50 mM HEPES-KOH, pH 7.6, 150 mM KCl, 1 mM EDTA, 1 mM Na_3VO_4 and 10% glycerol) (Loring et al., 2008). Yeast cells grown in YEPD at 24^{O}C were resuspended in 50 mM HEPES-KOH, pH 7.6, 150 mM KCl, 1 mM EDTA, 20 mM sodium pyrophosphate, 10 mM NaN3, 20 mM NaF, 1 mM Na_3VO_4, 100mM β-glycerophosphate, 0.5% OG, 10% glycerol, 1X Protease inhibitor cocktail (Sigma) and Complete EDTA-free protease inhibitor cocktail (Roche) and lysed with glass beads. GST and GST fusion protein bound beads were incubated with clarified yeast cell extracts for 1 hour at 4^{O}C with agitation. Beads were then washed with wash buffer. Bound proteins were analyzed via SDS-page, Gelcode Blue staining (Thermo Scientific) and by immunoblot.

For competition experiments, GST-Dma1 bound beads were first incubated with 0.5 mg peptides resuspended in 50 mM HEPES-KOH, pH 7.6, 150 mM KCl, 1 mM EDTA and 10% glycerol prior to incubation with yeast cell extracts.

In vivo ubiquitylation experiments

Cells were co-transformed with pVT102-*VAC17*-GFP and CUP1-myc-Ub plasmids. Myc-Ub expression was induced with 100μM $CuCl_2$ and cells were grown overnight. Vac17-GFP was immunoprecipitated as described above and analyzed via immunoblot using anti-myc antibodies (1:2,000; Cell Signaling).

Microscopy

To visualize vacuoles, cells were labeled with 12 μg FM4-64 in 250 μL media for 1 hour,

then washed twice and grown in 5 ml fresh media for one doubling time (2-3 hours). Live cell images were obtained on a DeltaVision Restoration system (Applied Precision) using an inverted epifluorescence microscope (IX-71; Olympus) with a charge-coupled device camera (Cool-SNAP HQ; Photometrics) and processed in Photoshop.

Whole Genome Sequencing

Wild-type and mutant backcross pools were derived from sporulation of diploid strain LWY10741, which was obtained by mating strains *vac22-1* and LWY3250 (wild-type). Construction of pooled libraries and analysis of the resulting Illumina sequencing data was performed as previously described (Birkeland et al., 2010). The filter for potential *vac22-1* mutations demanded that (i) the candidate mutation changed the coding of a yeast ORF, (ii) the mutation site was covered by at least three reads in both the wild-type and *vac22-1* mutant pools, (iii) all reads in the wild-type pool corresponded to the wild-type allele, and (iv) all reads in the mutant pool corresponded to the mutant allele. This filter yielded only the *dma1-G232R* mutation. We note that the *vac22-1* mutant pool was a low quality library with only 4-fold base coverage of the yeast genome. As a result, we cannot rule out that other potential candidate mutations were missed. However, based on the biological analysis of *dma1-G232R* it is likely to be the sole cause of the *vac22-1* phenotype.

Genetic Screens

Wildtype (LWY3250) cells transformed with pRS416-*VAC17-GFP* were grown in SC-Ura + 0.5% CA media. Cells were resuspended in 1 ml 0.1 M sodium phosphate buffer, pH 7.0. EMS (Sigma) was added to a final concentration of 36.18 mg/ml and cells were incubated at 24^{O}C for 1 hour (Burke et al., 2000). Cells were washed with ddH_20, then

washed twice with 5% sodium thiosulfate and were grown in SC-Ura+ 0.5% CA media for 12 hours. Mutants with elevated Vac17-GFP fluorescence were isolated via Fluorescence Activated Cell Sorting (FACS) and were plated on SC-Ura media. Microscopy and western blot analysis were used to confirm the elevation of Vac17 levels in these mutants.

Table S1. Yeast Strains Used in this Study.

Strain	Genotype	Source
LWY7235	*MATa, ura3-52, leu2-3,-112, his3-Δ200, trp1-Δ901, lys2-801, suc2-Δ9*	(Catlett and Weisman, 1998)
LWY5798	*MATa, ura3-52, leu2-3,-112, his3-Δ200, trp1-Δ901, lys2-801, suc2-Δ9, vac17Δ::TRP1*	(Tang et al., 2003)
LWY7664	*MATa, ura3-52, leu2-3,-112, his3-Δ200, trp1-Δ901, lys2-801, suc2-Δ9, vac17Δ::TRP1, MYO2-GFP::HIS3*	(Peng and Weisman, 2008)
LWY12269	*MATa, ura3-52, leu2-3,-112, his3-Δ200, trp1-Δ901, lys2-801, suc2-Δ9, GFP-TUB1::URA3, kar9Δ ::kan^r, SPC42-mCherry::HIS3*	This study
LWY12086	*MATα, ura3-52, leu2-3,-112, his3-Δ200, trp1-Δ901, lys2-801, suc2-Δ9, vac17Δ::TRP1, myo2Δ::TRP1 [pRS413-mCherry-MYO2]*	This study
LWY11102	*MATa, ura3-52, leu2-3,-112, his3-Δ200, trp1-Δ901, lys2-801, suc2-Δ9, dma1Δ::kan^r*	This study
LWY11125	*MATα, ura3-52, leu2-3,-112, his3-Δ200, trp1-Δ901, lys2-801, suc2-Δ9, dma2Δ::kan^r*	This study
LWY11156	*MATa, ura3-52, leu2-3,-112, his3-Δ200, trp1-Δ901, lys2-801, suc2-Δ9, dma1Δ::kan^r, dma2Δ::kan^r*	This study
LWY11269	*MATα, ura3-52, leu2-3,-112, his3-Δ200, trp1-Δ901, lys2-801, suc2-Δ9, vac17Δ::TRP1, dma1Δ::kan^r*	This study
LWY11389	*MATa, ura3-52, leu2-3,-112, his3-Δ200, trp1-Δ901, lys2-801, suc2-Δ9, dma1Δ::kan^r, dma2Δ::kan^r, VAC17-TAP::LEU2*	This study
LWY11524	*MATα, ura3-52, leu2-3,-112, his3-Δ200, trp1-Δ901, lys2-801, suc2-Δ9, dma1Δ::kan^r, dma2Δ::kan^r, vac17-F225S-TAP::LEU2*	This study
LWY11528	*MATα, ura3-52, leu2-3,-112, his3-Δ200, trp1-Δ901, lys2-801, suc2-Δ9, dma1Δ::kan^r, dma2Δ::kan^r, vac17-L221P-TAP::LEU2*	This study
LWY11507	*MATα, ura3-52, leu2-3,-112, his3-Δ200, trp1-Δ901, lys2-801, suc2-Δ9, dma1Δ::kan^r, dma2Δ::kan^r, vac17-T240A-TAP::LEU2*	This study
LWY11541	*MATa, ura3-52, leu2-3,-112, his3-Δ200, trp1-Δ901, lys2-801, suc2-Δ9, dma1Δ::kan^r, dma2Δ::kan^r, vac17-S222A-TAP::LEU2*	This study
LWY11687	*MATα, ura3-52, leu2-3,-112, his3-Δ200, trp1-Δ901, lys2-801, suc2-Δ9, dma1Δ::kan^r, dma2Δ::kan^r, vac17Δ::TRP1*	This study
LWY12966	*MATa, ura3-52, leu2-3,-112, his3-Δ200, trp1-Δ901, lys2-801, suc2-Δ9, DMA1-3xGFP::HIS3*	This study
LWY8195	*MATa, ura3-52, leu2-3,-112, his3-Δ200, trp1-Δ901, lys2-801, suc2-Δ9, pep4-Δ1137, vac17Δ::TRP1, myo2Δ::TRP1 [YCp50-MYO2]*	This study
MHY501	*MAT*α, *his3-Δ200, leu2-3, -112, ura3-52, lys2-801, trp1-1*	(Chen et al., 1993)
MHY1409	*MATα, his3-Δ200, leu2-3, -112, ura3-52, lys2-801, trp1-1, uba1-2*	(Swanson and Hochstrasser, 2000)
MHY605	*MATα, his3-11, leu2-3, -112, ura3-Δ5, pre1-1::can^R*	(Chen and Hochstrasser, 1996)
MHY952	*MATα, his3-Δ200, leu2-3, -112, ura3-52, lys2-801, trp1-1, doa3-delta1::HIS3 [YEpDOA3$_{LS}$][YCpUbDOA3ΔLS]*	(Chen and Hochstrasser, 1996)
MHY973	*MATα, his3-Δ200, leu2-3, -112, ura3-52, lys2-801, trp1-1, doa3-delta1::HIS3 [YEpDOA3$_{LS}$][YCpUbDOA3ΔLS-T76A]*	(Chen and Hochstrasser, 1996)
MHY1072	*MATa, his3-Δ200, leu2-3, -112, ura3-52, lys2-801, trp1-1, pup1::leu2::HIS3, pup3-Δ2::HIS3 [Ycplac22PUP1][Yeplac181PUP3]*	(Chen and Hochstrasser, 1996)

MHY1071	*MATa, his3-Δ200, leu2-3, -112, ura3-52, lys2-801, trp1-1, pup1::leu2::HIS3, pup3-Δ2::HIS3 [Ycplac22pup1-K58E] [Yeplac181pup3-E151K]*	(Chen and Hochstrasser, 1996)

Table S2. Plasmids Used in this Study.

Plasmid	Description	Ref.
pRS416-VAC17	CEN, URA3	(Tang et al., 2003)
pRS416-vac17-L221P	CEN, URA3	This study
pRS416-vac17-S222T	CEN, URA3	This study
pRS416-vac17-F225S	CEN, URA3	(Peng and Weisman, 2008)
pRS416-vac17-D237G	CEN, URA3	This study
pRS416-vac17-Q238R	CEN, URA3	This study
pRS416-vac17-S202A	CEN, URA3	This study
pRS416-vac17-S206A,S207A,S208A	CEN, URA3	This study
pRS416-vac17-S213A	CEN, URA3	This study
pRS416-vac17-S222A	CEN, URA3	This study
pRS416-vac17-T224A	CEN, URA3	This study
pRS416-vac17-S236A	CEN, URA3	This study
pRS416-vac17-T240A	CEN, URA3	This study
pRS416-vac17-S247A,T248A	CEN, URA3	This study
pRS416-VAC17-GFP	CEN, URA3	(Tang et al., 2006)
pRS416-vac17-L221P-GFP	CEN, URA3	This study
pRS416-vac17-S222A-GFP	CEN, URA3	This study
pRS416-vac17-F225S-GFP	CEN, URA3	(Peng and Weisman, 2008)
pRS416-vac17-T240A-GFP	CEN, URA3	This study
pRS413-mCherry-MYO2	CEN, HIS3	(Jin et al., 2011)
pRS416-vac17-ΔPEST-GFP	CEN, URA3	(Tang et al., 2006)
pRS416-DMA1	CEN, URA3	This study
pRS416-dma1-G232R	CEN, URA3	This study
pRS416-DMA1-GFP	CEN, URA3	This study
pRS416-Dma1-tdTomato	CEN, URA3	This study
pRS415-VAC17	CEN, LEU2	This study
pRS415-vac17-L221P	CEN, LEU2	This study
pRS415-vac17-S222A	CEN, LEU2	This study
pRS415-vac17-F225S	CEN, LEU2	This study
pRS415-vac17-T240A	CEN, LEU2	This study
pRS415-VAC17-GFP	CEN, LEU2	This study
pRS415-vac17-L221P-GFP	CEN, LEU2	This study
pRS415-vac17-S222A-GFP	CEN, LEU2	This study
pRS415-vac17-F225S-GFP	CEN, LEU2	This study
pRS415-vac17-T240A-GFP	CEN, LEU2	This study

pGEX4T-1 Dma1	Amp	This study
pGEX4T-1 Myo2 cargo-binding domain	Amp	This study
pRS416-dma1-I329R	CEN, URA3	This study
pRS416-dma1-I329R-GFP	CEN, URA3	This study
CUP1-myc-Ub	2μ, LEU2	This study
pVT102-Vac17-GFP	2μ, URA3	This study
pVT102-VAC17	2μ, URA3	This study

References

Arai, S., Noda, Y., Kainuma, S., Wada, I., and Yoda, K. (2008). Ypt11 functions in bud-directed transport of the Golgi by linking Myo2 to the coatomer subunit Ret2. Curr Biol *18*, 987-991.

Bartholomew, C.R., and Hardy, C.F. (2009). p21-activated kinases Cla4 and Ste20 regulate vacuole inheritance in Saccharomyces cerevisiae. Eukaryotic cell *8*, 560-572.

Bieganowski, P., Shilinski, K., Tsichlis, P.N., and Brenner, C. (2004). Cdc123 and checkpoint forkhead associated with RING proteins control the cell cycle by controlling eIF2gamma abundance. The Journal of biological chemistry *279*, 44656-44666.

Birkeland, S.R., Jin, N., Ozdemir, A.C., Lyons, R.H., Jr., Weisman, L.S., and Wilson, T.E. (2010). Discovery of mutations in Saccharomyces cerevisiae by pooled linkage analysis and whole-genome sequencing. Genetics *186*, 1127-1137.

Bobola, N., Jansen, R.P., Shin, T.H., and Nasmyth, K. (1996). Asymmetric accumulation of Ash1p in postanaphase nuclei depends on a myosin and restricts yeast mating-type switching to mother cells. Cell *84*, 699-709.

Boldogh, I.R., Nowakowski, D.W., Yang, H.C., Chung, H., Karmon, S., Royes, P., and Pon, L.A. (2003). A protein complex containing Mdm10p, Mdm12p, and Mmm1p links mitochondrial membranes and DNA to the cytoskeleton-based segregation machinery. Molecular biology of the cell *14*, 4618-4627.

Boldogh, I.R., Yang, H.C., Nowakowski, W.D., Karmon, S.L., Hays, L.G., Yates, J.R., 3rd, and Pon, L.A. (2001). Arp2/3 complex and actin dynamics are required for actin-based mitochondrial motility in yeast. Proceedings of the National Academy of Sciences of the United States of America *98*, 3162-3167.

Brennwald, P., Kearns, B., Champion, K., Keranen, S., Bankaitis, V., and Novick, P. (1994). Sec9 is a SNAP-25-like component of a yeast SNARE complex that may be the effector of Sec4 function in exocytosis. Cell *79*, 245-258.

Brooks, L., 3rd, Heimsath, E.G., Jr., Loring, G.L., and Brenner, C. (2008). FHA-RING ubiquitin ligases in cell division cycle control. Cell Mol Life Sci *65*, 3458-3466.

Burke, D., Dawson, D., Stearns, T., and Cold Spring Harbor Laboratory. (2000). Methods in yeast genetics : a Cold Spring Harbor Laboratory course manual, 2000 edn (Plainview, N.Y.: Cold Spring Harbor Laboratory Press).

Buvelot Frei, S., Rahl, P.B., Nussbaum, M., Briggs, B.J., Calero, M., Janeczko, S., Regan, A.D., Chen, C.Z., Barral, Y., Whittaker, G.R.*, et al.* (2006). Bioinformatic and comparative localization of Rab proteins reveals functional insights into the uncharacterized GTPases Ypt10p and Ypt11p. Molecular and cellular biology *26*, 7299-7317.

Catlett, N.L., Duex, J.E., Tang, F., and Weisman, L.S. (2000). Two distinct regions in a yeast myosin-V tail domain are required for the movement of different cargoes. The Journal of cell biology *150*, 513-526.

Catlett, N.L., and Weisman, L.S. (1998). The terminal tail region of a yeast myosin-V mediates its attachment to vacuole membranes and sites of polarized growth. Proceedings of the National Academy of Sciences of the United States of America *95*, 14799-14804.

Chahwan, R., Gravel, S., Matsusaka, T., and Jackson, S.P. (2013). Dma/RNF8 proteins are evolutionarily conserved E3 ubiquitin ligases that target septins. Cell cycle *12*, 1000-1008.

Chaturvedi, P., Sudakin, V., Bobiak, M.L., Fisher, P.W., Mattern, M.R., Jablonski, S.A., Hurle, M.R., Zhu, Y., Yen, T.J., and Zhou, B.B. (2002). Chfr regulates a mitotic stress pathway through its RING-finger domain with ubiquitin ligase activity. Cancer research *62*, 1797-1801.
Chen, P., and Hochstrasser, M. (1996). Autocatalytic subunit processing couples active site formation in the 20S proteasome to completion of assembly. Cell *86*, 961-972.
Chen, P., Johnson, P., Sommer, T., Jentsch, S., and Hochstrasser, M. (1993). Multiple ubiquitin-conjugating enzymes participate in the in vivo degradation of the yeast MAT alpha 2 repressor. Cell *74*, 357-369.
Desnos, C., Huet, S., and Darchen, F. (2007). 'Should I stay or should I go?': myosin V function in organelle trafficking. Biology of the cell / under the auspices of the European Cell Biology Organization *99*, 411-423.
Du, Y., Walker, L., Novick, P., and Ferro-Novick, S. (2006). Ptc1p regulates cortical ER inheritance via Slt2p. The EMBO journal *25*, 4413-4422.
Durocher, D., Henckel, J., Fersht, A.R., and Jackson, S.P. (1999). The FHA domain is a modular phosphopeptide recognition motif. Molecular cell *4*, 387-394.
Durocher, D., Taylor, I.A., Sarbassova, D., Haire, L.F., Westcott, S.L., Jackson, S.P., Smerdon, S.J., and Yaffe, M.B. (2000). The molecular basis of FHA domain:phosphopeptide binding specificity and implications for phospho-dependent signaling mechanisms. Molecular cell *6*, 1169-1182.
Estrada, P., Kim, J., Coleman, J., Walker, L., Dunn, B., Takizawa, P., Novick, P., and Ferro-Novick, S. (2003). Myo4p and She3p are required for cortical ER inheritance in Saccharomyces cerevisiae. The Journal of cell biology *163*, 1255-1266.
Eves, P.T., Jin, Y., Brunner, M., and Weisman, L.S. (2012). Overlap of cargo binding sites on myosin V coordinates the inheritance of diverse cargoes. The Journal of cell biology *198*, 69-85.
Fagarasanu, A., Fagarasanu, M., Eitzen, G.A., Aitchison, J.D., and Rachubinski, R.A. (2006). The peroxisomal membrane protein Inp2p is the peroxisome-specific receptor for the myosin V motor Myo2p of Saccharomyces cerevisiae. Developmental cell *10*, 587-600.
Fagarasanu, A., Mast, F.D., Knoblach, B., Jin, Y., Brunner, M.J., Logan, M.R., Glover, J.N., Eitzen, G.A., Aitchison, J.D., Weisman, L.S*., et al.* (2009). Myosin-driven peroxisome partitioning in S. cerevisiae. The Journal of cell biology *186*, 541-554.
Fagarasanu, A., Mast, F.D., Knoblach, B., and Rachubinski, R.A. (2010). Molecular mechanisms of organelle inheritance: lessons from peroxisomes in yeast. Nature reviews *11*, 644-654.
Fortsch, J., Hummel, E., Krist, M., and Westermann, B. (2011). The myosin-related motor protein Myo2 is an essential mediator of bud-directed mitochondrial movement in yeast. The Journal of cell biology *194*, 473-488.
Foth, B.J., Goedecke, M.C., and Soldati, D. (2006). New insights into myosin evolution and classification. Proceedings of the National Academy of Sciences of the United States of America *103*, 3681-3686.
Fraschini, R., Bilotta, D., Lucchini, G., and Piatti, S. (2004). Functional characterization of Dma1 and Dma2, the budding yeast homologues of Schizosaccharomyces pombe Dma1 and human Chfr. Molecular biology of the cell *15*, 3796-3810.
Fukuda, M., and Itoh, T. (2004). Slac2-a/melanophilin contains multiple PEST-like sequences that are highly sensitive to proteolysis. The Journal of biological chemistry *279*, 22314-22321.
Fukuda, M., Kuroda, T.S., and Mikoshiba, K. (2002). Slac2-a/melanophilin, the missing link between Rab27 and myosin Va: implications of a tripartite protein complex for melanosome transport. The Journal of biological chemistry *277*, 12432-12436.
Garcia-Rodriguez, L.J., Gay, A.C., and Pon, L.A. (2007). Puf3p, a Pumilio family RNA binding protein, localizes to mitochondria and regulates mitochondrial biogenesis and motility in budding yeast. The Journal of cell biology *176*, 197-207.

Ghaemmaghami, S., Huh, W.K., Bower, K., Howson, R.W., Belle, A., Dephoure, N., O'Shea, E.K., and Weissman, J.S. (2003). Global analysis of protein expression in yeast. Nature *425*, 737-741.
Grosshans, B.L., Andreeva, A., Gangar, A., Niessen, S., Yates, J.R., 3rd, Brennwald, P., and Novick, P. (2006). The yeast lgl family member Sro7p is an effector of the secretory Rab GTPase Sec4p. The Journal of cell biology *172*, 55-66.
Guertin, D.A., Venkatram, S., Gould, K.L., and McCollum, D. (2002). Dma1 prevents mitotic exit and cytokinesis by inhibiting the septation initiation network (SIN). Developmental cell *3*, 779-790.
Guo, W., Roth, D., Walch-Solimena, C., and Novick, P. (1999). The exocyst is an effector for Sec4p, targeting secretory vesicles to sites of exocytosis. The EMBO journal *18*, 1071-1080.
Hammer, J.A., 3rd, and Sellers, J.R. (2011). Walking to work: roles for class V myosins as cargo transporters. Nature reviews *13*, 13-26.
Hammer, J.A., 3rd, and Sellers, J.R. (2012). Walking to work: roles for class V myosins as cargo transporters. Nature reviews *13*, 13-26.
Huen, M.S., Grant, R., Manke, I., Minn, K., Yu, X., Yaffe, M.B., and Chen, J. (2007). RNF8 transduces the DNA-damage signal via histone ubiquitylation and checkpoint protein assembly. Cell *131*, 901-914.
Hwang, E., Kusch, J., Barral, Y., and Huffaker, T.C. (2003). Spindle orientation in Saccharomyces cerevisiae depends on the transport of microtubule ends along polarized actin cables. The Journal of cell biology *161*, 483-488.
Ikebe, M. (2008). Regulation of the function of mammalian myosin and its conformational change. Biochemical and biophysical research communications *369*, 157-164.
Ishikawa, K., Catlett, N.L., Novak, J.L., Tang, F., Nau, J.J., and Weisman, L.S. (2003). Identification of an organelle-specific myosin V receptor. The Journal of cell biology *160*, 887-897.
Itoh, T., Toh, E.A., and Matsui, Y. (2004). Mmr1p is a mitochondrial factor for Myo2p-dependent inheritance of mitochondria in the budding yeast. The EMBO journal *23*, 2520-2530.
Itoh, T., Watabe, A., Toh, E.A., and Matsui, Y. (2002). Complex formation with Ypt11p, a rab-type small GTPase, is essential to facilitate the function of Myo2p, a class V myosin, in mitochondrial distribution in Saccharomyces cerevisiae. Molecular and cellular biology *22*, 7744-7757.
Jaspersen, S.L., and Winey, M. (2004). The budding yeast spindle pole body: structure, duplication, and function. Annual review of cell and developmental biology *20*, 1-28.
Jin, Y., Sultana, A., Gandhi, P., Franklin, E., Hamamoto, S., Khan, A.R., Munson, M., Schekman, R., and Weisman, L.S. (2011). Myosin V transports secretory vesicles via a Rab GTPase cascade and interaction with the exocyst complex. Developmental cell *21*, 1156-1170.
Jin, Y., Taylor Eves, P., Tang, F., and Weisman, L.S. (2009). PTC1 is required for vacuole inheritance and promotes the association of the myosin-V vacuole-specific receptor complex. Molecular biology of the cell *20*, 1312-1323.
Johnson, A.E., and Gould, K.L. (2011). Dma1 ubiquitinates the SIN scaffold, Sid4, to impede the mitotic localization of Plo1 kinase. The EMBO journal *30*, 341-354.
Johnston, G.C., Prendergast, J.A., and Singer, R.A. (1991). The Saccharomyces cerevisiae MYO2 gene encodes an essential myosin for vectorial transport of vesicles. The Journal of cell biology *113*, 539-551.
Karcher, R.L., Roland, J.T., Zappacosta, F., Huddleston, M.J., Annan, R.S., Carr, S.A., and Gelfand, V.I. (2001). Cell cycle regulation of myosin-V by calcium/calmodulin-dependent protein kinase II. Science (New York, NY *293*, 1317-1320.
Karpova, T.S., Reck-Peterson, S.L., Elkind, N.B., Mooseker, M.S., Novick, P.J., and Cooper, J.A. (2000). Role of actin and Myo2p in polarized secretion and growth of Saccharomyces cerevisiae. Molecular biology of the cell *11*, 1727-1737.
Korinek, W.S., Copeland, M.J., Chaudhuri, A., and Chant, J. (2000). Molecular linkage underlying microtubule orientation toward cortical sites in yeast. Science (New York, NY *287*, 2257-2259.

Kvam, E., and Goldfarb, D.S. (2007). Nucleus-vacuole junctions and piecemeal microautophagy of the nucleus in S. cerevisiae. Autophagy *3*, 85-92.
Lee, L., Tirnauer, J.S., Li, J., Schuyler, S.C., Liu, J.Y., and Pellman, D. (2000). Positioning of the mitotic spindle by a cortical-microtubule capture mechanism. Science (New York, NY *287*, 2260-2262.
Lewandowska, A., Macfarlane, J., and Shaw, J.M. (2013). Mitochondrial association, protein phosphorylation, and degradation regulate the availability of the active Rab GTPase Ypt11 for mitochondrial inheritance. Molecular biology of the cell *24*, 1185-1195.
Liakopoulos, D., Kusch, J., Grava, S., Vogel, J., and Barral, Y. (2003). Asymmetric loading of Kar9 onto spindle poles and microtubules ensures proper spindle alignment. Cell *112*, 561-574.
Lillie, S.H., and Brown, S.S. (1994). Immunofluorescence localization of the unconventional myosin, Myo2p, and the putative kinesin-related protein, Smy1p, to the same regions of polarized growth in Saccharomyces cerevisiae. The Journal of cell biology *125*, 825-842.
Lipatova, Z., Tokarev, A.A., Jin, Y., Mulholland, J., Weisman, L.S., and Segev, N. (2008). Direct interaction between a myosin V motor and the Rab GTPases Ypt31/32 is required for polarized secretion. Molecular biology of the cell *19*, 4177-4187.
Liu, W., Santiago-Tirado, F.H., and Bretscher, A. Yeast formin Bni1p has multiple localization regions that function in polarized growth and spindle orientation. Molecular biology of the cell *23*, 412-422.
Long, R.M., Gu, W., Lorimer, E., Singer, R.H., and Chartrand, P. (2000). She2p is a novel RNA-binding protein that recruits the Myo4p-She3p complex to ASH1 mRNA. The EMBO journal *19*, 6592-6601.
Loring, G.L., Christensen, K.C., Gerber, S.A., and Brenner, C. (2008). Yeast Chfr homologs retard cell cycle at G1 and G2/M via Ubc4 and Ubc13/Mms2-dependent ubiquitination. Cell cycle (Georgetown, Tex *7*, 96-105.
Lu, H., Krementsova, E.B., and Trybus, K.M. (2006). Regulation of myosin V processivity by calcium at the single molecule level. The Journal of biological chemistry *281*, 31987-31994.
Mailand, N., Bekker-Jensen, S., Faustrup, H., Melander, F., Bartek, J., Lukas, C., and Lukas, J. (2007). RNF8 ubiquitylates histones at DNA double-strand breaks and promotes assembly of repair proteins. Cell *131*, 887-900.
Mao, K., and Klionsky, D.J. (2013). Mitochondrial fission facilitates mitophagy in Saccharomyces cerevisiae. Autophagy *9*.
Marchal, C., Haguenauer-Tsapis, R., and Urban-Grimal, D. (1998). A PEST-like sequence mediates phosphorylation and efficient ubiquitination of yeast uracil permease. Molecular and cellular biology *18*, 314-321.
Martinez, L.O., Agerholm-Larsen, B., Wang, N., Chen, W., and Tall, A.R. (2003). Phosphorylation of a pest sequence in ABCA1 promotes calpain degradation and is reversed by ApoA-I. The Journal of biological chemistry *278*, 37368-37374.
Mast, F.D., Rachubinski, R.A., and Dacks, J.B. (2012). Emergent complexity in Myosin V-based organelle inheritance. Molecular biology and evolution *29*, 975-984.
Michel, A.H., and Kornmann, B. (2012). The ERMES complex and ER-mitochondria connections. Biochemical Society transactions *40*, 445-450.
Miller, R.K., Cheng, S.C., and Rose, M.D. (2000). Bim1p/Yeb1p mediates the Kar9p-dependent cortical attachment of cytoplasmic microtubules. Molecular biology of the cell *11*, 2949-2959.
Moseley, J.B., and Goode, B.L. (2006). The yeast actin cytoskeleton: from cellular function to biochemical mechanism. Microbiol Mol Biol Rev *70*, 605-645.
Mulvihill, D.P., Pollard, P.J., Win, T.Z., and Hyams, J.S. (2001). Myosin V-mediated vacuole distribution and fusion in fission yeast. Curr Biol *11*, 1124-1127.
Murone, M., and Simanis, V. (1996). The fission yeast dma1 gene is a component of the spindle assembly checkpoint, required to prevent septum formation and premature exit from mitosis if spindle function is compromised. The EMBO journal *15*, 6605-6616.

Otzen, M., Rucktaschel, R., Thoms, S., Emmrich, K., Krikken, A.M., Erdmann, R., and van der Klei, I.J. Pex19p contributes to peroxisome inheritance in the association of peroxisomes to Myo2p. Traffic (Copenhagen, Denmark) *13*, 947-959.
Palmer, R.E., Sullivan, D.S., Huffaker, T., and Koshland, D. (1992). Role of astral microtubules and actin in spindle orientation and migration in the budding yeast, Saccharomyces cerevisiae. The Journal of cell biology *119*, 583-593.
Pashkova, N., Jin, Y., Ramaswamy, S., and Weisman, L.S. (2006). Structural basis for myosin V discrimination between distinct cargoes. The EMBO journal *25*, 693-700.
Peng, Y., and Weisman, L.S. (2008). The cyclin-dependent kinase Cdk1 directly regulates vacuole inheritance. Developmental cell *15*, 478-485.
Pruyne, D., and Bretscher, A. (2000). Polarization of cell growth in yeast. Journal of cell science *113 (Pt 4)*, 571-585.
Pruyne, D., Gao, L., Bi, E., and Bretscher, A. (2004a). Stable and dynamic axes of polarity use distinct formin isoforms in budding yeast. Molecular biology of the cell *15*, 4971-4989.
Pruyne, D., Legesse-Miller, A., Gao, L., Dong, Y., and Bretscher, A. (2004b). Mechanisms of polarized growth and organelle segregation in yeast. Annual review of cell and developmental biology *20*, 559-591.
Raspelli, E., Cassani, C., Lucchini, G., and Fraschini, R. (2011). Budding yeast Dma1 and Dma2 participate in regulation of Swe1 levels and localization. Molecular biology of the cell *22*, 2185-2197.
Roeder, A.D., Hermann, G.J., Keegan, B.R., Thatcher, S.A., and Shaw, J.M. (1998). Mitochondrial inheritance is delayed in Saccharomyces cerevisiae cells lacking the serine/threonine phosphatase PTC1. Molecular biology of the cell *9*, 917-930.
Rogers, S.L., Karcher, R.L., Roland, J.T., Minin, A.A., Steffen, W., and Gelfand, V.I. (1999). Regulation of melanosome movement in the cell cycle by reversible association with myosin V. The Journal of cell biology *146*, 1265-1276.
Rossanese, O.W., and Glick, B.S. (2001). Deconstructing Golgi inheritance. Traffic (Copenhagen, Denmark) *2*, 589-596.
Santiago-Tirado, F.H., Legesse-Miller, A., Schott, D., and Bretscher, A. (2011). PI4P and Rab inputs collaborate in myosin-V-dependent transport of secretory compartments in yeast. Developmental cell *20*, 47-59.
Scolnick, D.M., and Halazonetis, T.D. (2000). Chfr defines a mitotic stress checkpoint that delays entry into metaphase. Nature *406*, 430-435.
Sellers, J.R., and Knight, P.J. (2007). Folding and regulation in myosins II and V. Journal of muscle research and cell motility *28*, 363-370.
Seshan, A., and Amon, A. (2004). Linked for life: temporal and spatial coordination of late mitotic events. Current opinion in cell biology *16*, 41-48.
Shepard, K.A., Gerber, A.P., Jambhekar, A., Takizawa, P.A., Brown, P.O., Herschlag, D., DeRisi, J.L., and Vale, R.D. (2003). Widespread cytoplasmic mRNA transport in yeast: identification of 22 bud-localized transcripts using DNA microarray analysis. Proceedings of the National Academy of Sciences of the United States of America *100*, 11429-11434.
Sil, A., and Herskowitz, I. (1996). Identification of asymmetrically localized determinant, Ash1p, required for lineage-specific transcription of the yeast HO gene. Cell *84*, 711-722.
Sousa, M.J., Azevedo, F., Pedras, A., Marques, C., Coutinho, O.P., Preto, A., Geros, H., Chaves, S.R., and Corte-Real, M. (2011). Vacuole-mitochondrial cross-talk during apoptosis in yeast: a model for understanding lysosome-mitochondria-mediated apoptosis in mammals. Biochemical Society transactions *39*, 1533-1537.

Spellman, P.T., Sherlock, G., Zhang, M.Q., Iyer, V.R., Anders, K., Eisen, M.B., Brown, P.O., Botstein, D., and Futcher, B. (1998). Comprehensive identification of cell cycle-regulated genes of the yeast Saccharomyces cerevisiae by microarray hybridization. Molecular biology of the cell *9*, 3273-3297.
Strom, M., Hume, A.N., Tarafder, A.K., Barkagianni, E., and Seabra, M.C. (2002). A family of Rab27-binding proteins. Melanophilin links Rab27a and myosin Va function in melanosome transport. The Journal of biological chemistry *277*, 25423-25430.
Swanson, R., and Hochstrasser, M. (2000). A viable ubiquitin-activating enzyme mutant for evaluating ubiquitin system function in Saccharomyces cerevisiae. FEBS letters *477*, 193-198.
Tang, F., Kauffman, E.J., Novak, J.L., Nau, J.J., Catlett, N.L., and Weisman, L.S. (2003). Regulated degradation of a class V myosin receptor directs movement of the yeast vacuole. Nature *422*, 87-92.
Tang, F., Peng, Y., Nau, J.J., Kauffman, E.J., and Weisman, L.S. (2006). Vac8p, an armadillo repeat protein, coordinates vacuole inheritance with multiple vacuolar processes. Traffic (Copenhagen, Denmark) *7*, 1368-1377.
Terrak, M., Rebowski, G., Lu, R.C., Grabarek, Z., and Dominguez, R. (2005). Structure of the light chain-binding domain of myosin V. Proceedings of the National Academy of Sciences of the United States of America *102*, 12718-12723.
Theesfeld, C.L., Irazoqui, J.E., Bloom, K., and Lew, D.J. (1999). The role of actin in spindle orientation changes during the Saccharomyces cerevisiae cell cycle. The Journal of cell biology *146*, 1019-1032.
Trybus, K.M. (2008). Myosin V from head to tail. Cell Mol Life Sci *65*, 1378-1389.
Wagner, W., Brenowitz, S.D., and Hammer, J.A., 3rd (2011). Myosin-Va transports the endoplasmic reticulum into the dendritic spines of Purkinje neurons. Nature cell biology *13*, 40-48.
Weisman, L.S. (2006). Organelles on the move: insights from yeast vacuole inheritance. Nature reviews *7*, 243-252.
Weisman, L.S., and Wickner, W. (1988). Intervacuole exchange in the yeast zygote: a new pathway in organelle communication. Science (New York, NY *241*, 589-591.
Wickner, W. (2010). Membrane fusion: five lipids, four SNAREs, three chaperones, two nucleotides, and a Rab, all dancing in a ring on yeast vacuoles. Annual review of cell and developmental biology *26*, 115-136.
Win, T.Z., Gachet, Y., Mulvihill, D.P., May, K.M., and Hyams, J.S. (2001). Two type V myosins with non-overlapping functions in the fission yeast Schizosaccharomyces pombe: Myo52 is concerned with growth polarity and cytokinesis, Myo51 is a component of the cytokinetic actin ring. Journal of cell science *114*, 69-79.
Wu, J., Chen, Y., Lu, L.Y., Wu, Y., Paulsen, M.T., Ljungman, M., Ferguson, D.O., and Yu, X. Chfr and RNF8 synergistically regulate ATM activation. Nature structural & molecular biology *18*, 761-768.
Wu, X., Bowers, B., Rao, K., Wei, Q., and Hammer, J.A., 3rd (1998). Visualization of melanosome dynamics within wild-type and dilute melanocytes suggests a paradigm for myosin V function In vivo. The Journal of cell biology *143*, 1899-1918.
Wu, X.S., Rao, K., Zhang, H., Wang, F., Sellers, J.R., Matesic, L.E., Copeland, N.G., Jenkins, N.A., and Hammer, J.A., 3rd (2002). Identification of an organelle receptor for myosin-Va. Nature cell biology *4*, 271-278.
Yin, H., Pruyne, D., Huffaker, T.C., and Bretscher, A. (2000). Myosin V orientates the mitotic spindle in yeast. Nature *406*, 1013-1015.
Zheng, N., Wang, P., Jeffrey, P.D., and Pavletich, N.P. (2000). Structure of a c-Cbl-UbcH7 complex: RING domain function in ubiquitin-protein ligases. Cell *102*, 533-539.